National Renewable Energy Laboratory
A national laboratory of the U.S. Department of Energy
Office of Energy Efficiency & Renewable Energy
Innovation for Our Energy Future

Characterization and Analysis of CIGS and CdTe Solar Cells

December 2004 – July 2008

J.R. Sites
Colorado State University
Fort Collins, Colorado

Subcontract Report
NREL/SR-520-44811
January 2009

NREL is operated for DOE by the Alliance for Sustainable Energy, LLC Contract No. DE-AC36-08-GO28308

Characterization and Analysis of CIGS and CdTe Solar Cells

December 2004 – July 2008

J.R. Sites
Colorado State University
Fort Collins, Colorado

NREL Technical Monitor: Bolko von Roedern

Prepared under Subcontract No(s). XXL-5-44205-03

Subcontract Report
NREL/SR-520-44811
January 2009

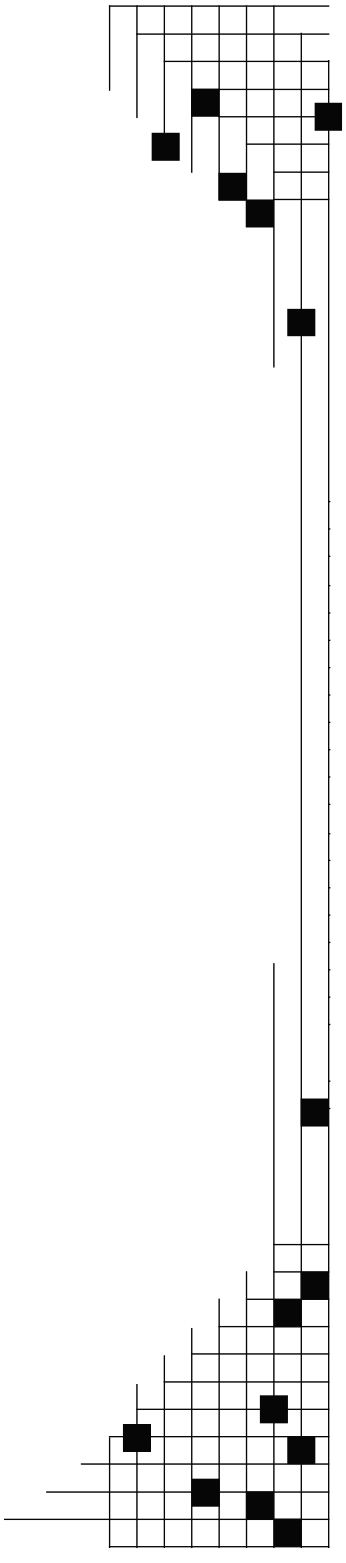

National Renewable Energy Laboratory
1617 Cole Boulevard, Golden, Colorado 80401-3393
303-275-3000 • www.nrel.gov

NREL is a national laboratory of the U.S. Department of Energy
Office of Energy Efficiency and Renewable Energy
Operated by the Alliance for Sustainable Energy, LLC

Contract No. DE-AC36-08-GO28308

SUMMARY

A number of studies relating to the fundamental operation of CIGS and CdTe solar cells were performed during the Subcontract period, and we have worked closely with industrial, university, and NREL partners to evaluate specific cells. In addition, we have expanded our LBIC (light-beam-induced-current) capabilities and the formalism needed to evaluate spatial non-uniformities, and we have analyzed the effective efficiency to be expected from commercial thin-film modules.

The fundamental work on CIGS cells included a detailed analysis of grain-boundary effects using two-dimensional modeling. It showed that the relatively benign effects observed are best explained by a decrease in the valence band edge in the vicinity of the grain boundary. A second project, which followed earlier work relating spatial grading of CIGS to performance, showed the increasing importance of an electron reflector at the back of the CIGS absorber as it is made progressively thinner. A third project generalized earlier work on the window/absorber conduction band offset to show that there is a general rule governing when a "spike" leads to a distortion of the current-voltage curve.

The CdTe studies included calculations of what could be done to increase voltage above current levels, the analytical consequences of small absorber lifetimes, and an explanation of how different combinations of absorber lifetime and back-contact barrier lead to different common features seen with CdTe cells. Additional projects extended stability and uniformity studies to focus on performance differences among cells with various back contacts and yielded a reasonably convincing explanation of the 1.456-eV photoluminescence peak from CdTe as a copper-oxygen donor complex about 150 meV below the conduction-band minimum.

TABLE OF CONTENTS

FIGURES

INTRODUCTION

The work reported here embodies a device-physics approach based on careful measurement and interpretation of data from $CuIn_{1-x}Ga_xSe_2$ (CIGS) and CdTe solar cells. The project goals have been to (1) reliably and quantitatively separate individual performance loss mechanisms, (2) expand the tools available for such measurement and analysis, (3) refine the physical explanations for performance losses, and (4) suggest fabrication approaches or modifications that can reduce these losses.

The experimental and analytical work for this project was largely done by a dedicated group of research students. The eight students who completed their PhD degrees during the Subcontract period have all actively contributed to the photovoltaic community since their graduation:

Alex Pudov, Nanosolar (CIGS)

Markus Gloeckler, First Solar (CdTe)

Samuel Demtsu, SoloPower (CIGS), PrimeStar (CdTe)

Caroline Corwine, Advent Solar (thin Si)

Tim Nagle, CSIRO Australia (dye sensitized)

Ana Kanevce, NREL (HIT, multijunction III-V)

Jun Pan, CSU (CdTe, CIGS)

Alan Davies, AVA Solar (CdTe)

The titles of their theses, the other students involved, and the Subcontract publications and presentations are all listed in the final section of the report. In addition to the new group of PhD scientists, we are very pleased that former PhD graduates Ingrid Repins and Jennifer Granata have now joined the photovoltaic programs at NREL and Sandia respectively.

BASIC CIGS STUDIES

CIGS Grain Boundaries. Probably the most important CIGS subcontract project was the calculations to show why grain boundaries in CIGS cells are sufficiently benign to allow the large voltages and efficiencies observed. Markus Gloeckler, in collaboration with Wyatt Metzger at NREL, modeled the CIGS grain boundary (GB) by a thin layer located between two uniform regions of CIGS material. The results summarized here were published in the Journal of Applied Physics **98**, 113704 (2005).

Figure 1 below shows the basic structure used for simulation of vertical GBs. The mesh spacing used for numerical solutions of the Poisson equation was varied so that it is finer in regions where rapid changes in parameters are expected. The GB region was modified in various ways, but a baseline three-layer (ZnO/CdS/CIGS) structure was assumed otherwise, and the GB differed from the surrounding material only by the presence of additional defects or by an expansion of the band gap. The results were not sensitive to the width of the GB layer so long as it is in the range of 2 to 50 nm.

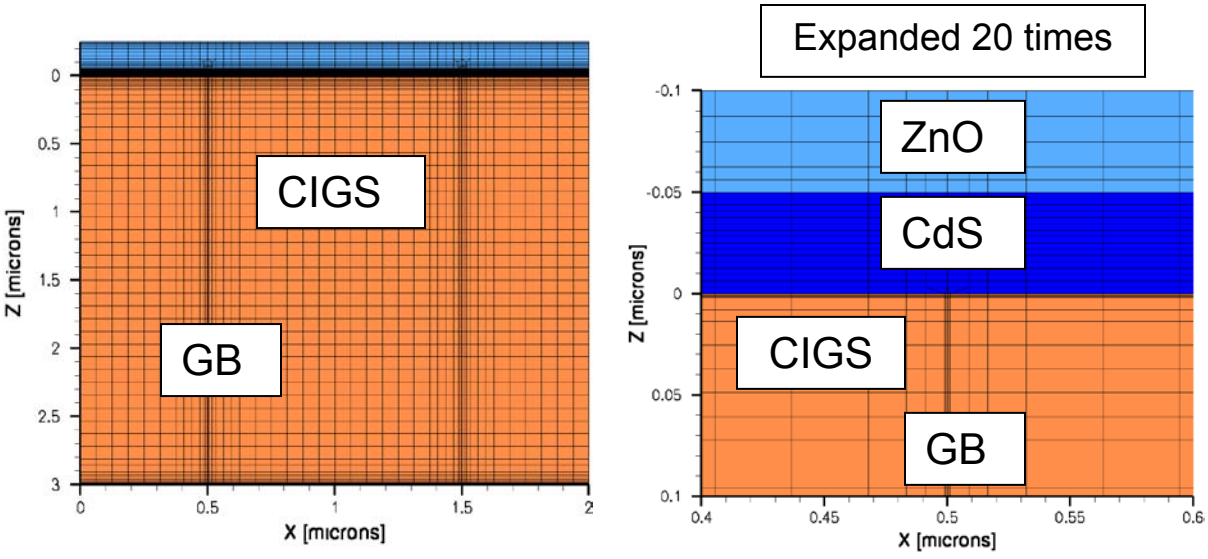

Figure 1. Simulation mesh used for CIGS vertical grain-boundary calculations.

Three physical types of columnar GBs, as well as combinations, were considered: an increased density of defects at a neutral GB, a charge sheet at the GB, and an expansion

of the valence band in the GB region. In all cases, a spacing of 1 micron between GBs was assumed. In the first case, the GB recombination velocity S_{gb} was used as the primary parameter. The simulation results in Fig. 2 show a decline in all parameters, but the most dramatic is in voltage. The conclusion is that S_{gb} must be the order of 1000 cm/s or less for neutral GBs to be benign. This would imply nearly complete passivation, which seems unlikely for GBs in CIGS. The results shown in Fig. 2 are in good agreement with those of Taretto et. al. [Thin Solid Films **480-481**, 8 (2005)].

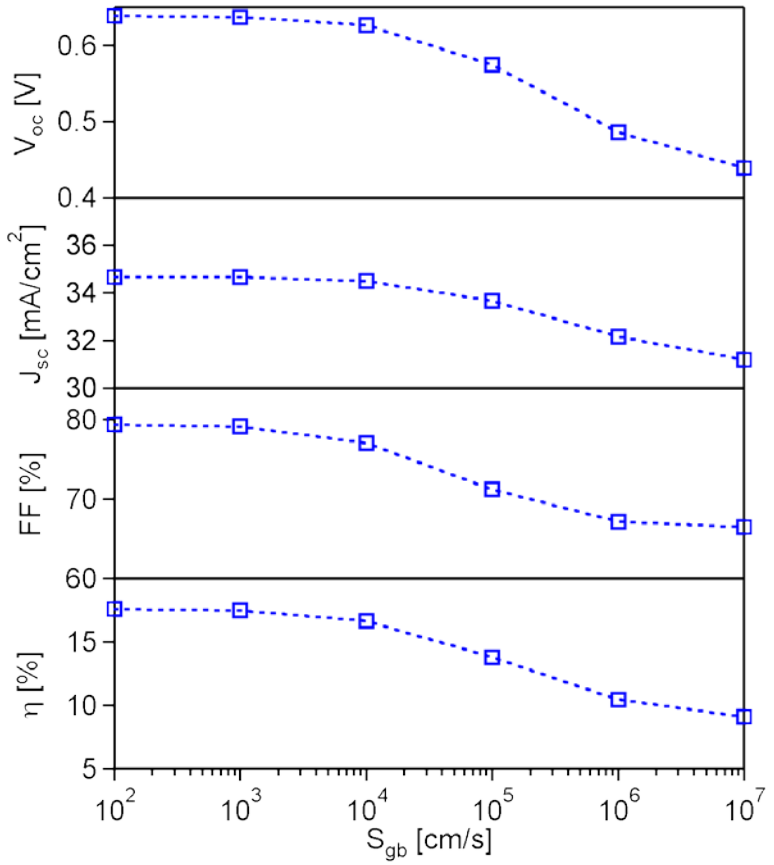

Figure 2. Effect of neutral GB recombination on columnar GBs. Lower limit of S_{gb} is the absence of GBs.

The second GB possibility explored was a sheet of positive charge, and hence a potential φ_{gb}, created by GB defects. This scenario is appealing, because it implies hole repulsion from the GB region, and hence larger current collection. In fact, we predict a current increase of as much as 4 mA/cm^2 for charge potentials above 0.4 eV. The counterpoint, however, is that as the GB potential is increased, the quasi-Fermi levels for electrons and

holes become closer to each other, or equivalently, there is an increasing region where n and p approach the same order of magnitude. This situation will substantially increase forward recombination and reduce the open-circuit voltage. Physically, the same potential that assists collection by channeling the photogenerated electrons and holes will, in forward bias, provide channels for electrons and holes to flow in the opposite direction, allow greater recombination, and hence increase the forward current and reduce V_{OC}.

The dual effects of the charge potential on collection and forward-current enhancement are shown in Fig. 3. The top reference line is the baseline with no GBs. The lower reference line corresponds to a GB recombination velocity S_{gb} of 10^5 cm/s and no charge potential. As φ_{gb} increases, the voltage (upper left) goes down and somewhat later the current (upper right) goes up. The fill-factor (lower left) changes very little. The combined effect on efficiency (lower right) is an initial decrease from the neutral recombination value and a latter increase as the collection effect becomes significant. Efficiency, however, never approaches the GB-free, or GB-benign, condition.

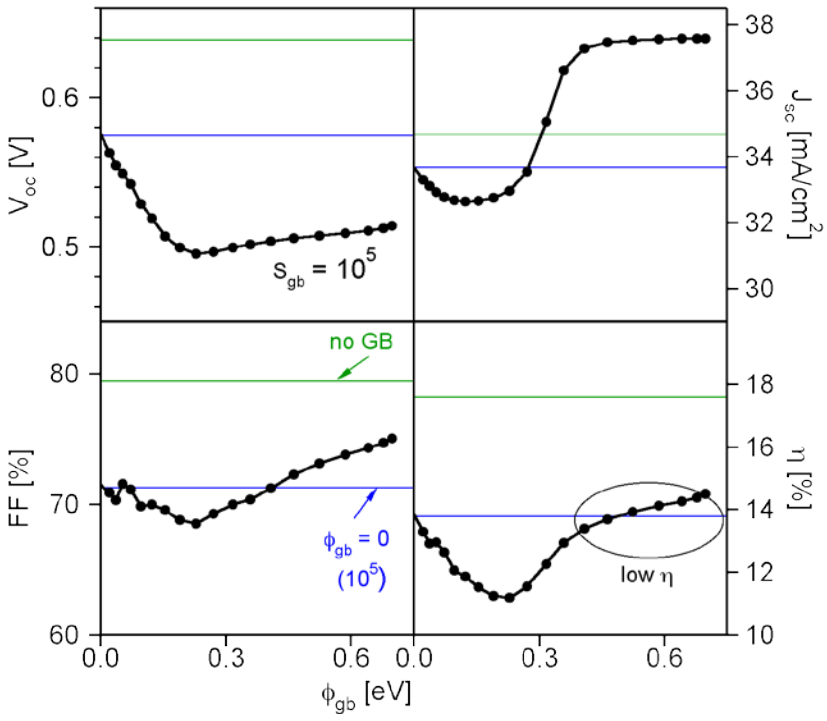

Figure 3. Current-voltage parameters as a function of GB charge potential assuming S_{gb} is 10^5 cm/s.

The possibility of a valence-band expansion near CIGS GBs was the third major scenario considered. There is both experimental [Hetzer et.al., APL **86**, 162105 (2005)] and theoretical [Persson and Zunger, PRL **91**, 266401 (2003)] evidence for such an increase as a result of copper depletion near CIGS GBs. As implied in Fig. 4, holes will be kept away from the GB, but additional electrons near the GB that would enhance the forward current will not be present. The simulated results for the solar-cell parameters are shown in Fig. 4.

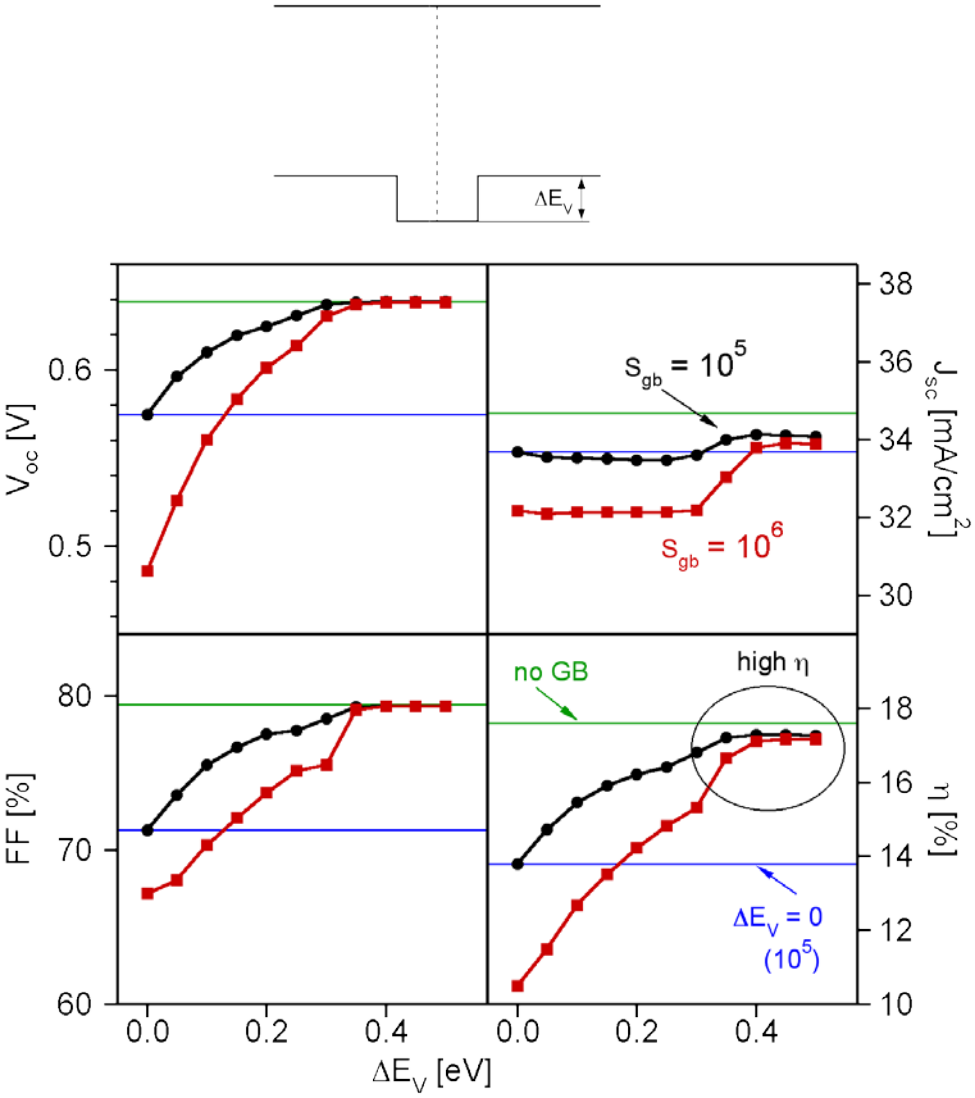

Figure 4. Current-voltage parameters as a function of valence band expansion ΔE_V.

The two reference lines from Fig. 3 are also used in Fig. 4. In this case, the voltage and fill-factor increase significantly as the valence-band hole barrier is increased until they

saturate at the GB-free values for ΔE_V greater than 0.3 eV. When $\Delta E_V = 0$, voltage and fill-factor vary significantly with S_{gb}, but as ΔE_V is increased, they converge to the GB-free value of S_{gb} and yield very nearly the GB-free efficiency. The current is always slightly lower, because fewer electron-hole pairs are generated in the expanded band-gap region near the GBs, but the net result is high efficiency.

If there is both a charge sheet and an expanded band gap at the GB, the ΔE_V curves in Fig. 4 are modified, but only slightly, by the charge sheet. Hence, the expanded band gap is the likely explanation for the benign character of grain boundaries in CIGS solar cells, and the degree of neutral-GB recombination and magnitude of the charge potential are predicted to play relatively minor roles.

Thin CIGS Absorbers. There are several advantages to reducing CIGS absorber thickness. However, one would generally expect the efficiency to decrease at smaller absorber thicknesses. Several groups have shown this to be the case for CIGS cells [Negami et al, Proc. 2nd WCPEC (1998) p. 1181; Lundberg et al, Prog. Photovoltaics **11**, 77 (2003); Ramanathan et al, Proc. 4th WCPEC (2006) p. 380]. Simulations carried out by Ana Kanevce (Fig. 5) showed decreases in the solar-cell parameters at small thicknesses. Her baseline case is based on Ramanathan's 1-μm result and is shown with circles. The minority-carrier lifetime in the absorber was taken to be 1 ns and the hole density 2 x 10^{16} cm^{-3}. At thicknesses less than 1 μm, all three solar-cell parameters decrease, and the rate of the decrease becomes steeper for thickness below 500 nm.

The calculated performance with an order of magnitude lower lifetime (squares in Fig. 5) has lower efficiency at 1-μm and higher thicknesses, but a less pronounced thickness dependence except at the extremely low thicknesses (< 400 nm). Variations in minority-carrier lifetime affect thicker devices more strongly than thin ones due to their larger recombination volume. A smaller hole-density (dots in Fig. 5) also decreases the voltage, but it increases the current by about the same fraction. Below 500 nm, the calculated efficiency is be nearly independent of lifetime and hole density.

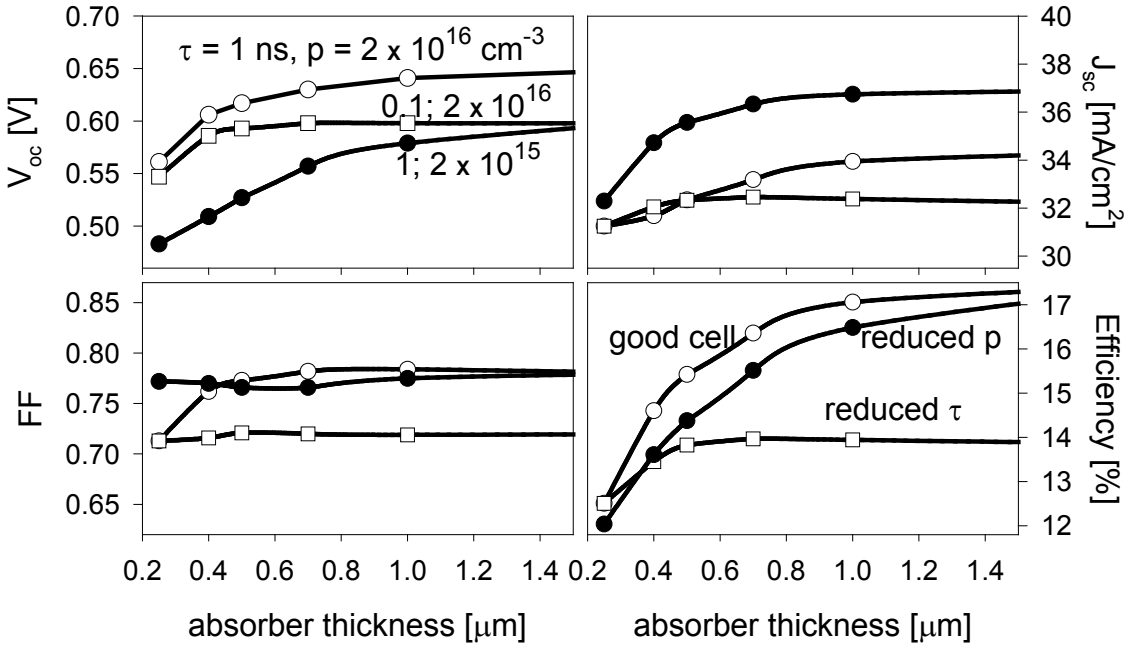

Figure 5. Calculated impact of absorber thickness on high-efficiency cell parameters (circles). Corresponding results with reduced lifetime (squares) and reduced carrier density (dots) also shown.

Earlier, Gloeckler and Sites [J. Appl. Phys. **98**, 103703 (2005)] showed that a key strategy for CIGS cells with absorber thicknesses below 1 μm is to limit back-contact recombination, which can be accomplished by an appropriate choice of back-contact material, surface modifications, or inclusion of grading in the Ga to In ratio. Fig. 6 shows that the inclusion of a simple electron reflector should substantially increase V_{oc} for thin devices. The electron reflector reduces the dominant minority-electron recombination at the back contact by keeping electrons away from it.

The dashed lines in Fig. 6 are for a constant band-gap absorber, and are similar to the baseline circles in Fig. 5. As seen in Fig. 6, efficiency is increased to essentially the same curve whether the reflector is formed by a band-gap expansion (increased Ga) localized at the back contact, or whether band-gap grading is spread over half or all of the absorber. (There is, however, a tradeoff between current and voltage when the average band gap is increased.) The recombination rate should be reduced by the same factor as the suppression of electron concentration, $\exp(\Delta E_{Ba}/kT)$, where ΔE_{Ba} is the band-gap

increase at the back contact. A back grading with a band-gap increase greater than 0.2 eV reduces recombination by a factor greater than 10^3. In this situation, V_{oc} is again limited by bulk recombination, and a larger barrier height does not further increase efficiency. As the absorber is thinned, the bulk volume and hence the bulk recombination decreases, and V_{oc} may actually be larger than that of thick devices.

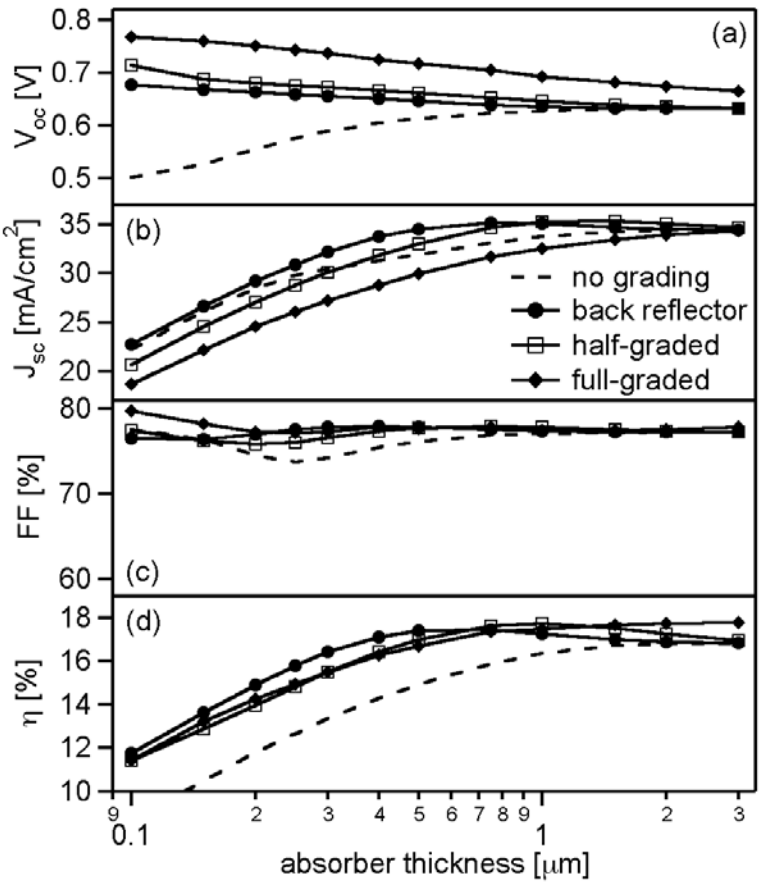

Figure 6. Performance parameters for the three grading profiles in comparison with an ungraded absorber (dashed line). ΔE_{Ba} = 0.2 eV.

Another aspect of thin CIGS layers is the possibility of back-side illumination. With illumination from the rear, the absorber thickness needs to be less than 1 μm for reasonable efficiency. Nakada et al [Proc. 20th EPSEC, 2005, p. 1736] showed experimentally that such efficiencies can in fact be achieved when a transparent back conductor is combined with a thin absorber. The major difference between illumination from the front and the back is the distribution of photogenerated carriers within the cell.

With front illumination, generation occurs primarily within the space-charge region (SCR), but with back illumination, most carriers are generated in the bulk part of the absorber, and most of those close to the back contact. Hence, back-contact recombination can be a very significant loss. That loss, however, can be significantly decreased through the choice of back-contact material and/or by increasing the Ga/In ratio, and hence the band gap, at the back of the device to produce the electron reflector.

Figure 7 shows Ana Kanevce's comparative simulations of standard solar-cell parameters for front and back illumination (circles and dots). The simulation parameters were taken from those of a high-efficiency thick cell with a 0.2-eV back-contact electron barrier. Also shown in the efficiency plot are the data reported by Nakada et al for front and back illumination. The dashed-line fits to that data would require that the absorber lifetime be reduced by a factor of ten from that of high-efficiency thick cells.

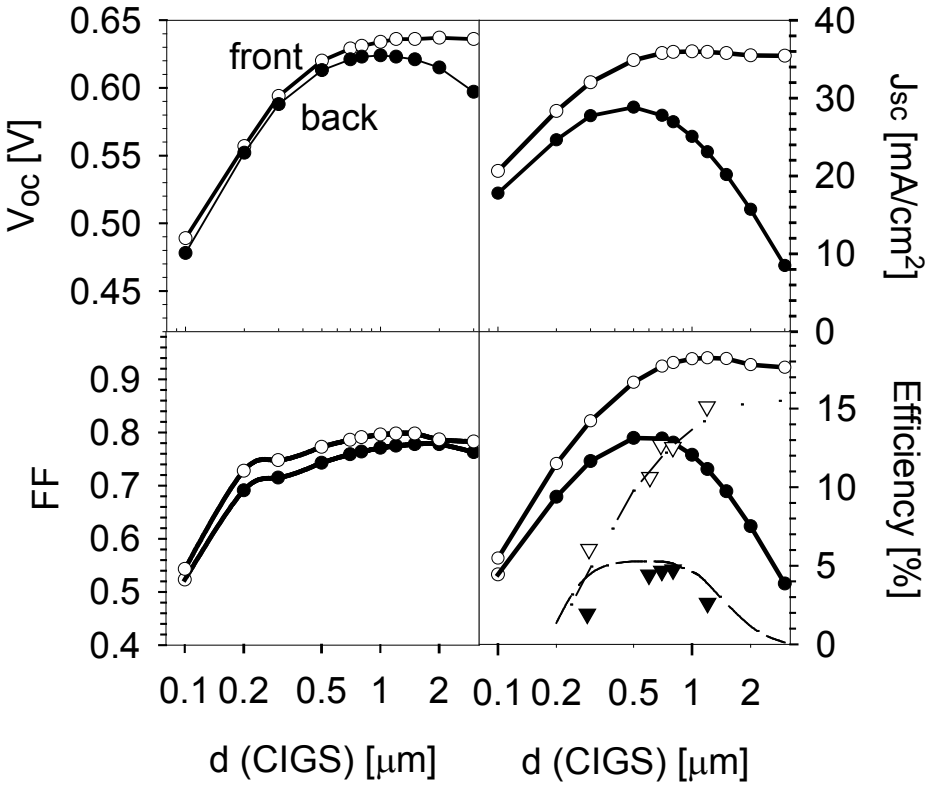

Figure 7. Variation in calculated J-V parameters with absorber thickness for front (circles) and back (dots) illumination. A back electron reflector is assumed. Experimental efficiency for front (open triangles) and back (filled triangles) illumination fit by dashed lines.

Three general features to note in Fig. 7 are (1) the shape of the experimental data, particularly the back-illumination efficiency peak near 0.7 μm, is similar to that seen in the calculations, (2) the very thin-film limit (below 0.2 μm), where the front- and back-illumination curves converge to the same values, and (3) the very large front/back-illumination difference seen in current for cells thicker than 0.5 μm.

Conduction-Band-Offset Rule. Ana Kanevce, with assistance from Markus Gloeckler, deduced the basic condition, and a very simple rule, governing when a positive conduction-band offset ("spike") leads to a distortion of the current-voltage curve. This work, which built on Alex Pudov's thesis work [A.O. Pudov, A. Kanevce, J.R. Sites, F. Hasoon, and H. Al-Thani, J. Appl. Phys, **97**, 064901 (2005)], was presented at the Spring 2005 MRS meeting [MRS Proc. **865**, 221 (2005)].

Figure 8 shows the band diagram of a CdS/CIS cell at zero bias, though the discussion could apply equally well to other windows and absorbers. Two features are critical: the conduction-band offset (CBO) ΔE_c and the splitting of the Fermi level under illumination into E_{Fn} for electrons, E_{Fp} for holes. Hole current has little influence on J-V distortion, and hence only the conduction band and quasi-Fermi level for electrons were analyzed.

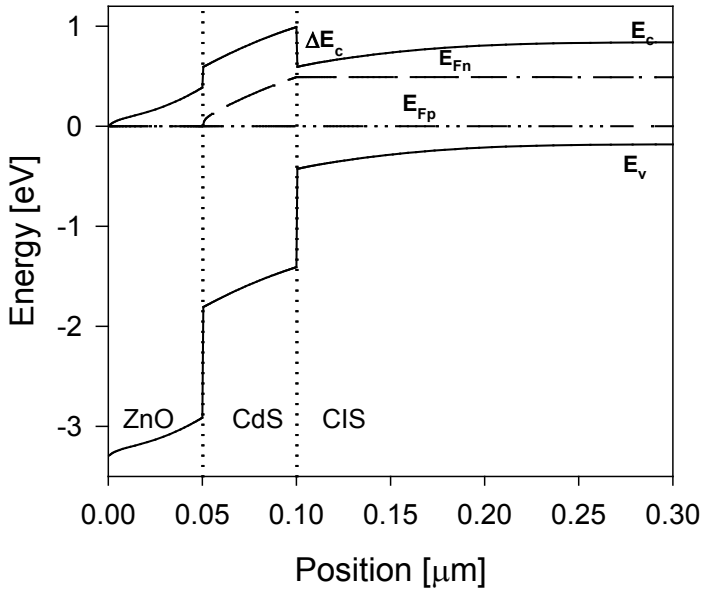

Figure 8. Band diagram for CdS/CIGS under illumination at zero bias.

Assuming thermionic emission across the CdS/CIS interface, the electron current density can be calculated by integrating over the product of carrier density and carrier velocities in the direction of transport v_x . The carrier densities are similar to the thermal velocity, so the integral can be simplified:

$$J_n = q\int_{E_c}^{\infty} v_x dn \approx qnv_{th} \quad ,$$

where v_{th} is the thermal velocity of electrons ~10^7 cm/s, q is the elementary charge, and n is the free carrier density given by:

$$n = N_c \exp[-\frac{E_c - E_{Fn}}{kT}].$$

N_c is the effective density of states in the conduction band, k is the Boltzmann constant, and T is the absolute temperature. Thus, at a fixed temperature, the maximum electron current through the junction is determined by n(CdS) and therefore by the energy difference between the conduction band and quasi-Fermi level for electrons in the CdS close to the interface with CIS or CIGS. An increase of this energy difference will result in fewer free electrons, and hence in a possible current limitation.

A typical photocurrent density achieved for CdS/CI(G)S cells is J_L = 32 mA/cm^2. According to equation (1), the minimum carrier density to provide the current flow would be n = 2x10^{10} cm^{-3}, which corresponds to a 0.48-eV difference between the conduction band and the quasi-Fermi level. If E_c - E_{Fn} exceeds this value, which is more likely for CIS or for small Ga concentration, additional drift fields are required to insure carrier transport across the barrier. This effectively places the main junction in forward bias, which reduces the CI(G)S depletion width and the current collection. For a large E_c - E_{Fn} difference, the transport becomes severely limited and collection effectively goes to zero. The 0.48-eV value depends on the particular choice of parameters used in the model. A different effective mass, for example, will alter the 0.48-eV value, but only weakly, since it appears in a logarithmic term. Similarly, the dependence on J_L is weak. At lower temperatures, however, the value of E_c - E_{Fn} that leads to the J-V distortion will be proportionally smaller.

E_{Fn} at the CdS/CI(G)S junction will depend in large part on the thickness and defect density of the CdS layer. As a concrete example, Fig 9 shows the calculated J-V curves from a CIS cell assuming a CdS/CIS band offset of 0.4 eV. As the CdS defect density is increased from the 10^{16} to the 10^{17} cm^{-3} range, the 0.48-eV line is crossed, and the distortion becomes severe. The bottom part of Fig. 10 divides the defect-density/CdS-thickness plane into three regions with reductions in V_{MP} the order of 0, 0.05, and 0.45 V.

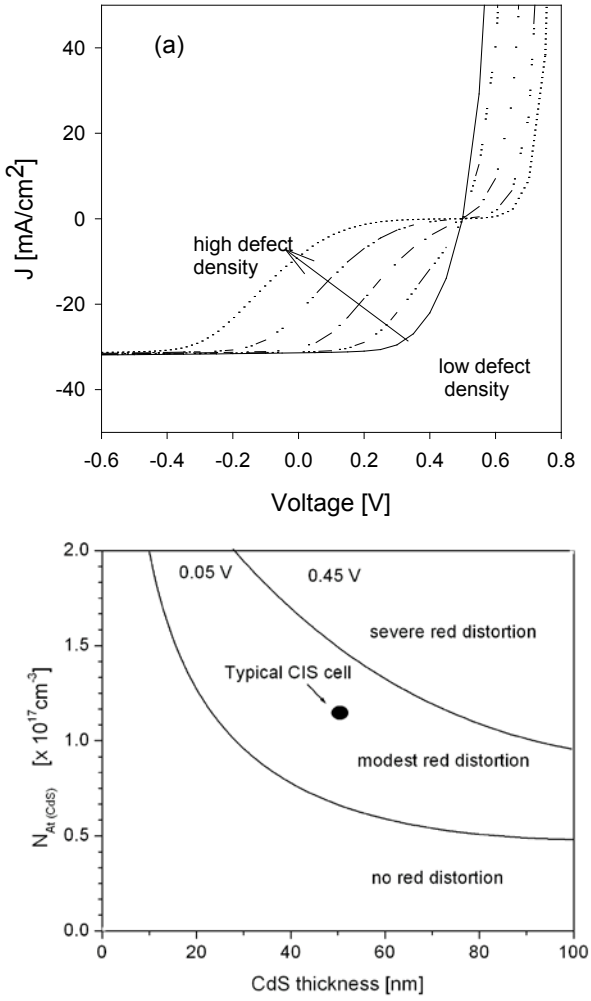

Figure 9. J-V dependence on CdS defect density (top); Variation in qualitative amount of distortion with N_{At} (midgap acceptor trap density in CdS) and CdS thickness (bottom).

High-Effiency CdZnS/CIGS. Ana also worked with Raghu Bhattacharya of NREL on the analysis of CIGS cells that that were fabricated with a solution-grown CdZnS buffer

layer. The best of these cells achieved 19.5% efficiency, equal to that achieved with NREL's standard CdS buffer on an absorber from the same depostion. At short wavelengths, the CdZnS buffer did achieve current about 2 mA/cm^2 higher than the CdS buffer, but it had slightly less collection in the longer-wavelength region. The CdZnS buffer also produced a slightly higher A-factor (1.5 vs. 1.3) both light and dark, and its C-V curve was slightly less well behaved and indicated a smaller CIGS carrier density near the junction. A more complete report can be found in Bhattacharya et al, Appl. Phys. Lett. **89**, 253503, (2006).

Laser-Assisted Deposition. A three-way collaboration with Tokio Nakada of Aoyama Gakuin University, Sho Shiraka of Ehime University, and Ana Kanevce at CSU explored several aspects of CIGS cells fabricated at AGU with laser-assisted deposition (LAD) of the absorber layer. Sho and Ana analyzed the impact of LAD on current-voltage, capacitance-voltage, and LBIC (light-beam-induced-current) measurements. Two LAD and one non-LAD cells which exhibited the best solar cell performance among 10 cells fabricated on one substrate were selected for more detailed analysis.

The conversion efficiencies of the best cells were in the 15-16% range, and the band gap varied between 1.21 and 1.27 eV. The series resistance in all cases was below 1 Ω-cm^2, and the leakage was below 1 mS/cm^2. The diode quality factors were between 1.65 and 1.9 with a lower A-factor and less QE loss in the red when the band gap was smaller. All of the cells experienced dark/light crossover in their current-voltage curves, but the crossover was considerably diminished when the dark curves followed a light soak of 1 minute. In this case, the full crossover was restored after 30 minutes in the dark. In general, the performance of the LAD cells was similar to the non-LAD cells. Capacitance-voltage measurements showed hole densities in the high 10^{15} cm^{-3} range with no systematic difference between LAD and non-LAD fabrication. LBIC also showed no significant differences in the LAD cells. Although obvious LAD effects were not observed with this cell set, research in this area will continue and will likely involve a more aggressive approach to LAD.

BASIC CdTe STUDIES

Voltage Deficit. The highest reported efficiency for thin-film CdTe cells lags that of thin-film CIGS solar cells by more than 3%. Based on band-gap considerations, one would predict a 3% difference in the opposite direction. The lower CdTe efficiency is primarily the result of a much larger voltage deficit between CdTe cells and crystalline cells of similar band gap.

Figure 10 compares J-V curves from record-effiency CIGS and CdTe cells with those of high-efficiency single-crystal Si and GaAs. The Si and GaAs curves were mathematically adjusted slightly (30-40 mV in voltage and about 1 mA/cm^2 in current density) for consistency with the CIGS and CdTe band gaps.

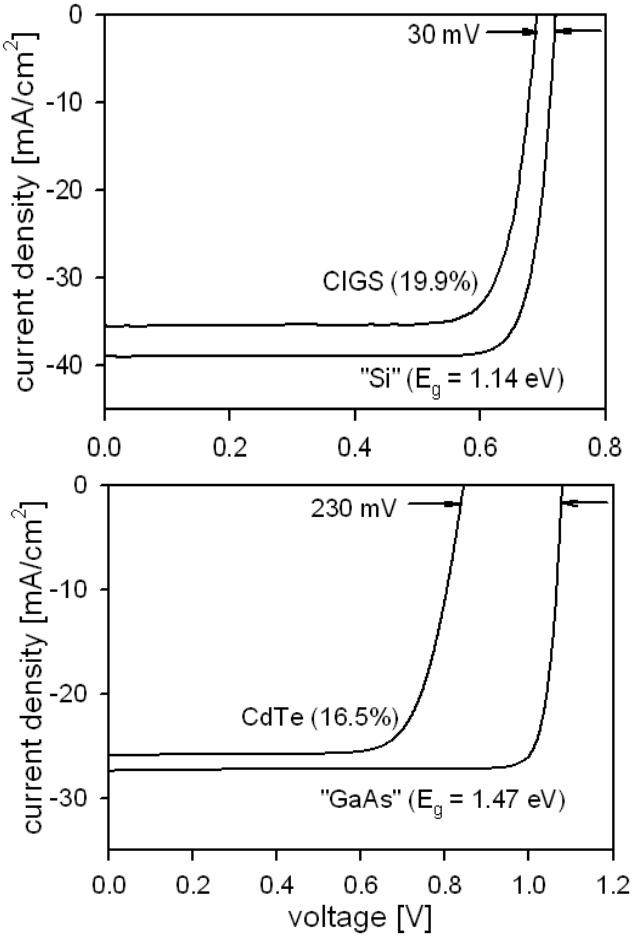

Figure 10. J-V Comparison of record CIGS cell with high-efficiency Si, adjusted slightly for band gap (top). Similar comparison of CdTe with GaAs (bottom).

The salient feature of Fig. 10 is the 230-mV voltage deficit for CdTe compared to the 30 mV deficit for CIGS. The CIGS voltage deficit is in fact remarkably small, and our explanation for the near-single-crystal behavior was discussed above. If it were possible to reduce the CdTe deficit to that of CIGS, the CeTe cell efficiency would increase by about 5% to approximately 22%. The obvious question is what might be done to significantly reduce the CdTe deficit.

Two distinctly different approaches for increasing CdTe voltage, which will be referred to as the "n-p" and the "n-i-p" strategies and depicted in Fig. 11, were examined. Figure 11a shows the band diagram of a CdTe solar cell with a thin n-CdS window layer.

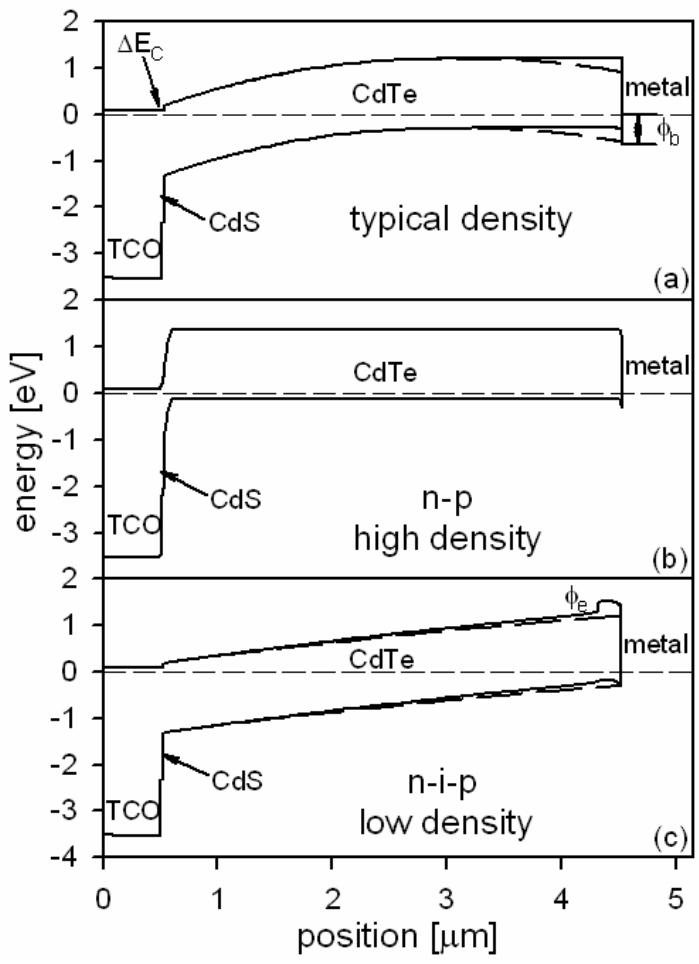

Figure 11. (a) Typical CdS/CdTe band diagram with and without a back-contact barrier. (b) Significantly higher hole density. (c) Lower density with and without an electron reflector.

The low CdTe hole density ($2x10^{14}$) in Fig. 11a is typical of today's cells and makes the CdTe absorber intermediate between i-type (intrinsic) and p-type. As a consequence, the depletion region extends over a large fraction, but not necessarily all, of the CdTe thickness. The possibility of a significant back-contact barrier Φ_b is indicated by the dashed line. Figure 11b, where the hole density is increased to $2x10^{17}$, is the classic n-p hetero-junction. It is similar to what one would find with n-on-p GaAs. In contrast, Fig. 11c lowers the hole density to $2x10^{13}$, the CdTe becomes fully depleted, and terminology used here is n(CdS)-i(CdTe)-p(back of CdTe). This configuration can also lead to high voltage, but of major importance in this case is the presence of an electron reflector Φ_e at the rear on the absorber.

CdTe-cell voltage was calculated by Jun Pan as a function of the CdTe recombination lifetime τ for the three situations shown in Fig. 11. Figure 12 shows graphically that both high lifetime and high carrier density would be required for a high voltage in the n-p configuration. Physically, a reduction in the density of defects could be the key to improvements in both: increased lifetime through a smaller number of recombination centers and increased carrier density through a smaller number of compensating states.

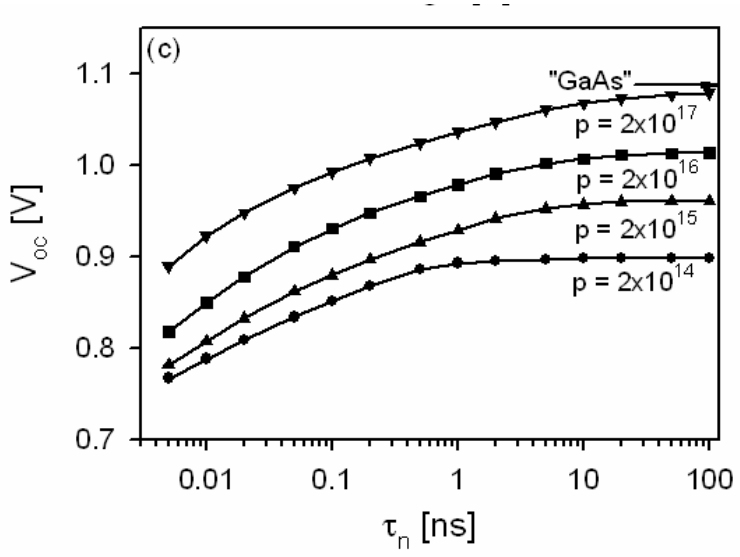

Figure 12. CdTe n-p cell needs major increases in both carrier density and lifetime.

Calculated voltages for the p = $2x10^{13}$ fully-depleted absorber configuration (Fig. 12c) are shown in Fig 13. In this case, a conduction-band barrier near the back surface, often

referred to as an electron reflector, is critical to reduce voltage-limiting recombination at the back surface. Without this increase, denoted Φ_e, the voltage is slightly lower than CdTe with a typical $2x10^{14}$ carrier-density, but with even a small back reflector (0.2 eV), the voltage should increase significantly. Higher values of Φ_e lead to only modest additional improvement, and the choice of thickness and carrier density of the reflector layer lead to only minor variations in the J-V curves.

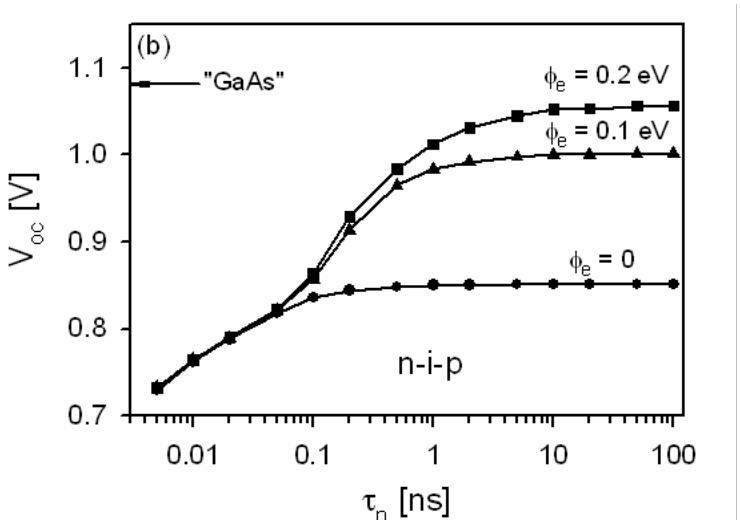

Figure 13. CdTe n-i-p requires a back electron reflector and modest lifetime.

Figure 13 shows that when the electron-reflector barrier is present, the lifetime need not be particularly high. One possibility for creating such a barrier is to add a layer of ZnTe, or perhaps CdZnTe, with an expanded gap in the conduction-band direction. A potential difficulty, however, is that any recombination at the CdTe/ZnTe or other reflector interface will compromise the advantage of keeping electrons away from the metal interface. If an electron barrier is applied to CdTe that is not fully depleted, the benefit is smaller, because one not have field collection throughout.

Figure 14 summarizes the two approaches to increasing CdTe voltage. The simulated n-p J-V curve corresponds to very substantial increases in CdTe lifetime and hole density. As shown, the n-p curve would have a voltage of 1080 mV and an efficiency of 22% even if current losses in today's record cell were not reduced. The n-i-p simulation yields a somewhat similar J-V curve with a voltage of 1030 mV and an efficiency of 21% at a moderate lifetime of 2 ns. It does require an electron reflector the order of 0.2 eV in

height near the back contact. It may well be the more promising strategy for improving voltage and performance, since it should not require a major improvement in the quality of thin-film CdTe to reach one volt and 20%.

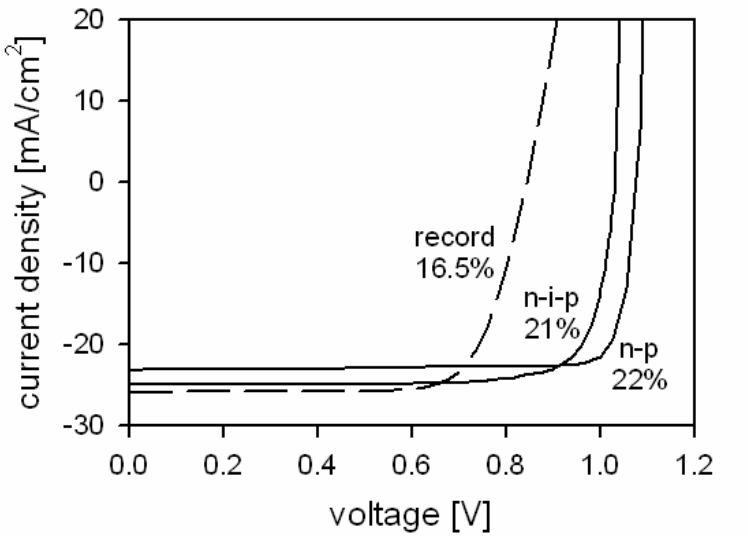

Figure 14. Comparison of record-cell J-V curve with possible major improvements using n-p and n-i-p strategies

Absorber Lifetime. The minority carrier lifetime of CdTe, which was the key parameter for the voltage calculations shown in Figs. 12 and 13, also has a strong influence on the solar-cell fill-factor (Fig. 15). From Jun Pan's calculations, the short-lifetime collection of photogenerated carriers, even those generated within the depletion region's electric field, is increasingly incomplete in forward voltage where the field is reduced. At higher lifetimes, essentially all carriers generated in the depletion region will be collected, and hence the dependence of collection on voltage becomes very small.

One analytical consequence of the low-lifetime curves in Fig. 15 is that they are no longer exponential, and the calculation of a well defined diode quality A fails. If one ignores the non-exponential behavior and attempts to calculate A, the voltage-dependent collection inherently overestimates its value. The result is shown in Fig. 16 where A = 1, light and dark, for large lifetimes where the forward diode current results from thermionic emission. At smaller lifetimes, bulk recombination becomes significantly larger, and the A-factor should transition to a Shockley-Reed-Hall value of 2, or slightly less if the

distribution of recombination states varies though the absorber. This is the case in the dark, where the J-V curve is unaffected by changes in photocarrier collection with voltage. In the light, however, the voltage-dependent-collection effect on the J-V curves yields artificial A-values well above 2 for the very short lifetimes and artificially enhanced A-values for typical CdTe-cell lifetimes.

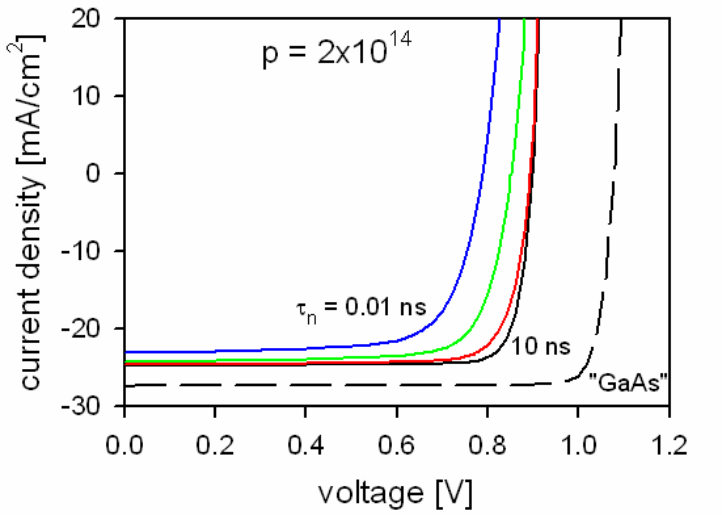

Figure 15. Calculated J-V for typical-carrier-density CdTe as a function of minority carrier lifetime, again referenced to GaAs prediction.

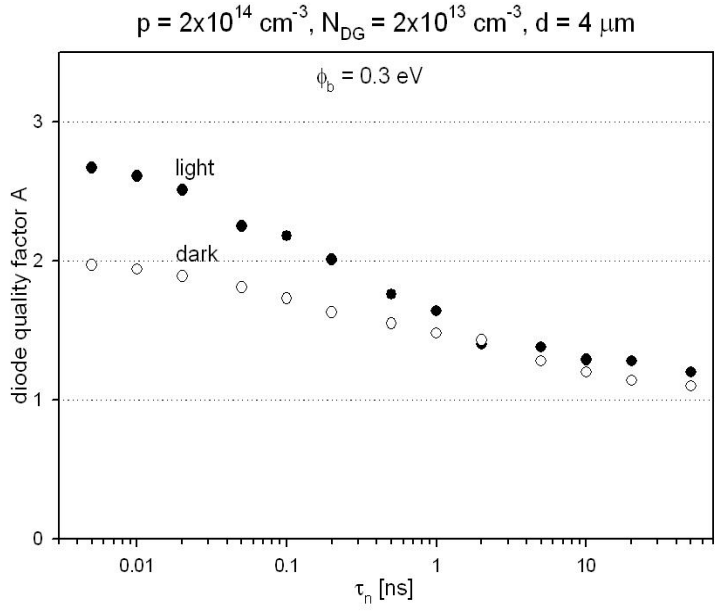

Figure 16. Artificial enhancement of A-factor in the light at small lifetimes.

Experimental curves from cells with different CdTe lifetimes are shown in Fig. 17. The measurements were made by Samuel Demtsu working in collaboration with David Albin at NREL. In this case, the lifetime variations result from different amounts of copper used in the formation of the back contact. There is, however, more than one effect seen in Fig. 17. With no copper at all, the back-contact barrier is significant, and thus the curve rolls over in the first quadrant and the fill-factor is reduced. With a small amount of copper, the back barrier is reduced, and the J-V curve is quite good. With additional copper, however the absorber lifetime is reduced, and the fill-factor is again smaller.

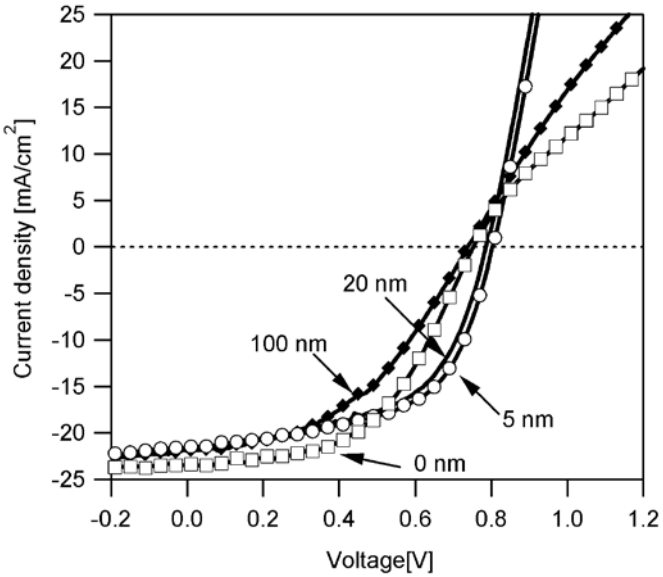

Figure 17. CdTe J-V curves for cells with different amounts of back-contact copper.

Reasonable values for experimental lifetimes can be deduced from time-resolved photoluminescence (TRPL) measurements. TRPL measurements from the same cells depicted in Fig. 17 were made by Wyatt Metzger at NREL and are shown in Fig. 18. Room-temperature capacitance-voltage measurements, also made on the same cells, showed an increase in net carrier density and a decrease in depletion width with increased amounts of Cu. Hence, we conclude that the use of copper helps the cell by reducing the back barrier, but it also introduces additional acceptors accompanied by a decrease in hole lifetime. A minimal amount of copper appears to be optimal for efficiency.

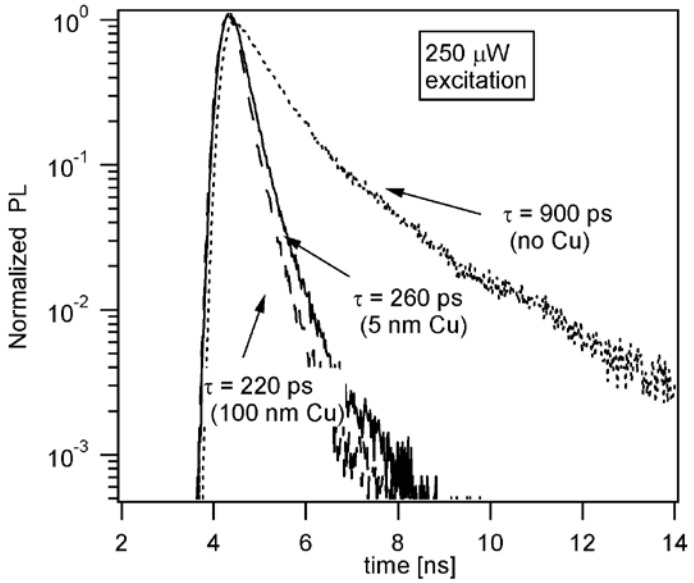

Fig. 18. Normalized CdTe TRPL decay curves as a function of the Cu amount.

Non-standard J-V Features. Jun Pan and Markus Gloeckler [J. Appl. Phys., 2006] investigated the combined effects of the back-contact barrier ϕ_b and variations in absorber carrier density. They showed that competing mechanisms can alter the *J-V* characteristics in two different ways. One is a majority-carrier (hole) limitation to forward current that also reduces fill-factor. The second is a high minority-carrier (electron) contribution to the forward current that results in reduced open-circuit voltage. CdTe solar cells are particularly prone to the latter, since the combination of a wide depletion region and impedance of light-generated holes at the back contact increases electron injection at the front diode. Characteristic J-V curves for four combinations of τ and ϕ_b are shown in Fig. 19.

Variations in *J-V* curves with carrier lifetime in the absence of a significant back barrier. Fig. 19(a) and (b), similar to Fig. 15, have a straightforward interpretation. In Fig. 19(a), low lifetime results in more recombination in the space-charge region (SCR) and, therefore, a higher forward current and hence lower V_{oc} and fill factor. Larger CdTe lifetimes will both reduce the forward current due to SCR recombination and increase the forward flow of electrons to the back contact. The net result, shown in Fig. 19(b), is a

significant increase in fill factor, with *A* approaching 1, but little effect on voltage.

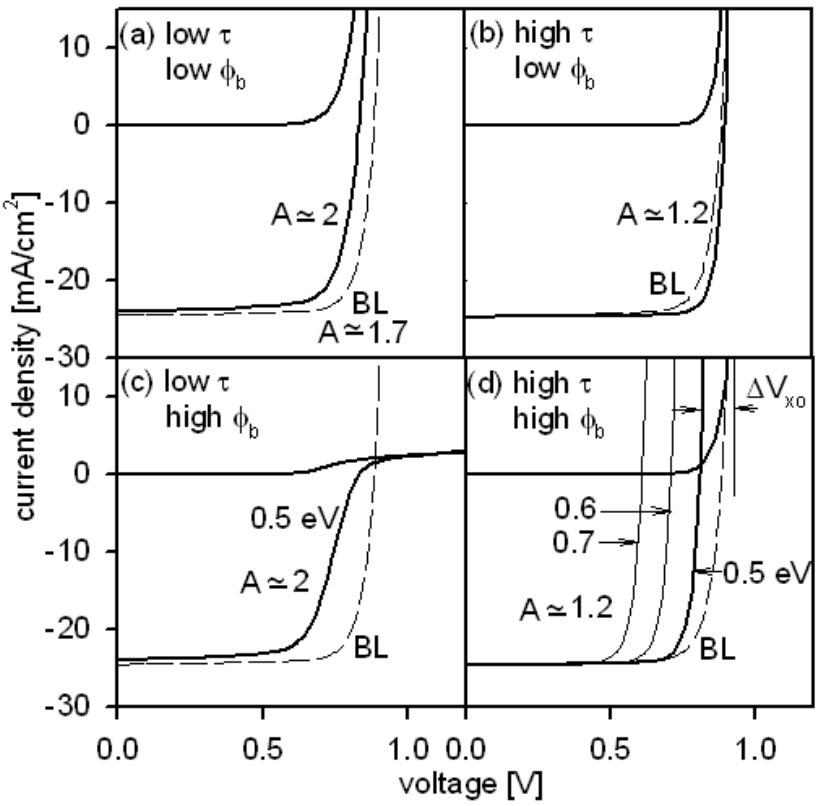

Figure 19. Calculated J-V curves for increasing and decreasing CdTe lifetime by a factor of ten and varying back-contact barrier. Baseline (BL) shown for reference.

Current-voltage curves similar to those shown in Fig. 19(c) are frequently observed for CdTe solar cells, and are attributed to impedance of hole current by the back barrier. The dark curve is nearly flat, because the hole current is limited by the Schottky back contact. The light curve appears relatively normal in the power quadrant, but with some loss in fill factor. Above V_{oc}, the light curve is also nearly flat. Commonly, however, the light curve saturates at a higher current than the dark curve, resulting in a crossover of light and dark *J-V* curves. The current limitation of both dark and light curves in the first quadrant is often referred to as rollover.

The illuminated *J-V* curves shown in Fig. 19(d) are somewhat counterintuitive, because they show a lower V_{oc} even though the lifetime is very high and the absorber is not fully depleted. V_{oc} decreases further with still higher back-barriers (also shown at ϕ_b = 0.6 eV

and 0.7 eV), and the *J-V* curves show substantial crossover between light and dark curves. For both dark and light conditions, the quasi-Fermi level for electrons is much closer to the conduction band than it is for low CdTe lifetime. This simply means that the electron density is high throughout the CdTe, and one can expect enhanced electron current. The total current of the diode is dominated by the back-contact electron recombination current, which increases with a larger barrier and reduces V_{oc}. For larger barriers, in fact, the incremental reduction in V_{oc} is equal to the increase in ϕ_b. Overlap of front and back space-charge regions will always enhance electron current, but it is not a requirement for substantially increased forward current.

CdTe Stability. Samuel Demtsu and Alan Davies, in collaboration with David Albin and Joel Pankow at NREL, [Solar Energy Mat. Solar Cells, 2006] investigated the stability and performance of CdS/CdTe solar cells made using four different back contact structures. Two device sets were made with Ag and Ni deposited on a Cu-doped graphite layer. For the other two sets, the graphite layer was removed before the application of the Ag or Ni. Figure 20 shows the changes in parameters when a typical cell in each category was held for extended periods of time at 100°C under open-circuit bias and one-sun illumination.

Devices made with graphite/Ag and graphite/Ni back contacts showed similar initial performance, and modest degradation under stress. In the presence of a graphite layer, no measurable difference in performance or stability was seen between the use of Ag or Ni as a secondary contact. In this configuration, the graphite paste behaves like a diffusion barrier. In the absence of the graphite layer, devices made with Ni-only and Ag-only back contacts, had significantly smaller FF initially, and showed much faster degradation than those with the graphite layer. Degradation was predominantly due to a decrease in FF. For the Ag-only back contact device, diffusion of Ag from the back contact resulted in higher CdTe doping concentrations before and after stress. Fast Ag diffusion along grain boundaries also contributed to shunt formation and increased the micro non-uniformity. For Ni-only devices, the Ni alloyed with the Te-rich CdTe surface forming Ni_3Te_2.

Though the Ni_3Te_2 intermetallic layer helps minimize Ni diffusion, shunting can result from the formation of micro non-uniformities in these devices, relative to the more stable graphite-layer devices.

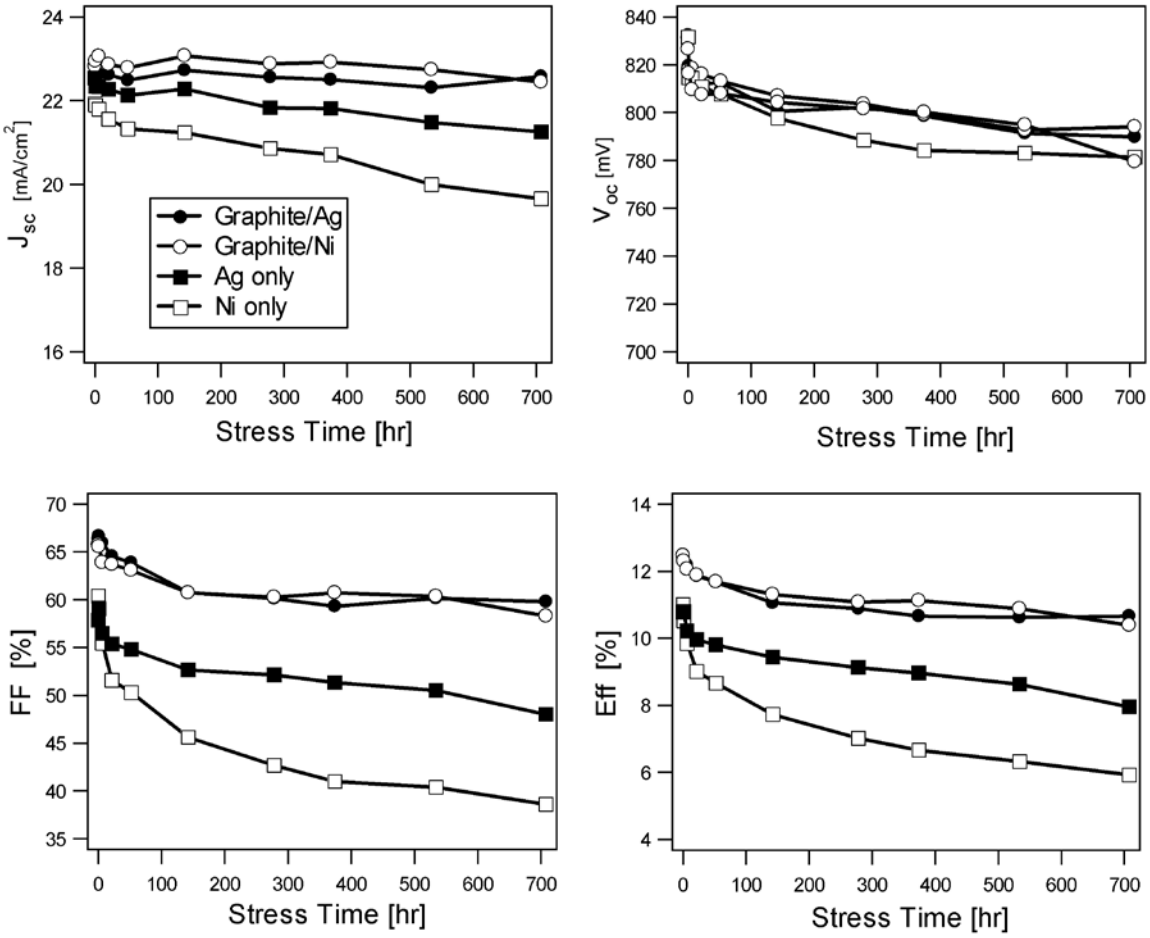

Figure 20. J-V parameters vs. stress time at 100°C, one sun, and open-circuit voltage for cells made with four types of back contact.

Light-beam-induced current (LBIC) measurements before and after stress showed little change in spatial uniformity for devices with a graphite layer, but they did show increased variations of 6% and 2% respectively for the Ag-only and Ni-only devices. This increase in non-uniformity reflects the formation of micro non-uniformities when these devices were stressed. The poorer collection of carriers is likely explained by ohmic micro-shunts, or possibly by increased recombination due to larger defect concentrations in the CdTe and CdS layers.

Thin CdS. Several thin-film CdS/CdTe solar cells were fabricated with Prof. Sampath's in-line CSS pilot deposition line at Colorado State University. Quantum efficiency measurements were performed by Alan Davies to ascertain CdS layer thicknesses, identify the degree of CdS/CdTe intermixing (small), and estimate the absorber band-gap (about 1.47 eV for all of the cells). QE curves for eight devices (Fig. 21) show the variation in CdS thickness among thedevices sampled. From the QE data in the 400-500 nm range, we estimated optical CdS thicknesses ranging from about 10 to 240 nm. Also evident from QE curves is a modest decrease in collection of photogenerated carriers in the thinner CdS cells for wavelengths near the band-gap. This decrease can reasonably be attributed to a shorter electron lifetime for thin-CdS devices

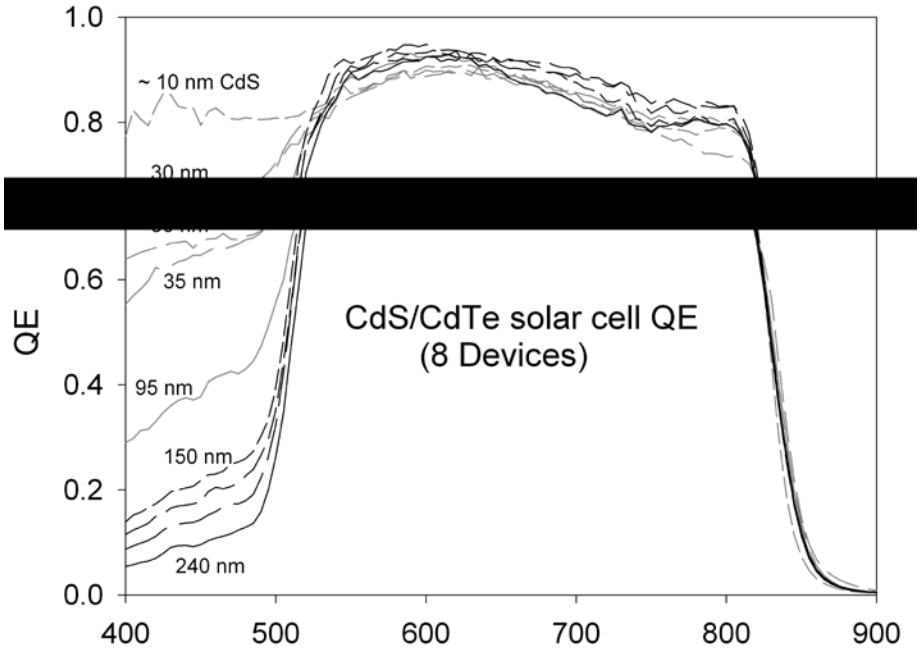

Figure 21: Variation of CdS/CdTe QE response with CdS thickness.

Figure 22 shows all three J-V parameters for the same cells used for the Fig. 22 QE curves. Efficiencies, which are between 10 and 12% for devices with thicker CdS, fall into the 3 to 6% range once the CdS thickness is significantly below 100 nm. Immediately evident is the increase in J_{sc} with thinner CdS resulting from the increased transmission as CdS is thinned. Also obvious is the sharp drop in V_{OC} and increase in J_o between 100 and 50 nm. As CdS thickness decreases, CdS pin-hole formation is likely to

become more prevalent, and consequently J_o and V_{OC} would approach values that may correspond to a SnO_2/CdTe photodiode.

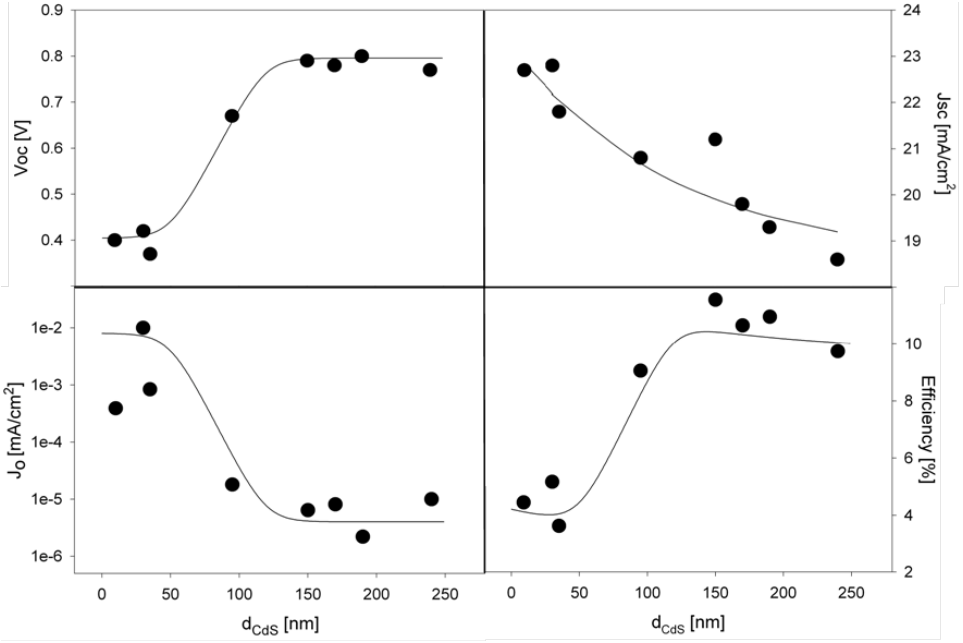

Figure 22: J-V parameters, plotted against CdS layer thickness, show overall performance loss below 100 nm.

The concept of pinholes exposing the CdTe directly to the SnO_2 window layer strongly suggests that the thin-CdS cells should have a significantly less uniform photovoltaic response. This predicted contrast in uniformity is clearly seen in the Fig. 23 LBIC scans, which show a broadening of local QE distribution by about twenty times.

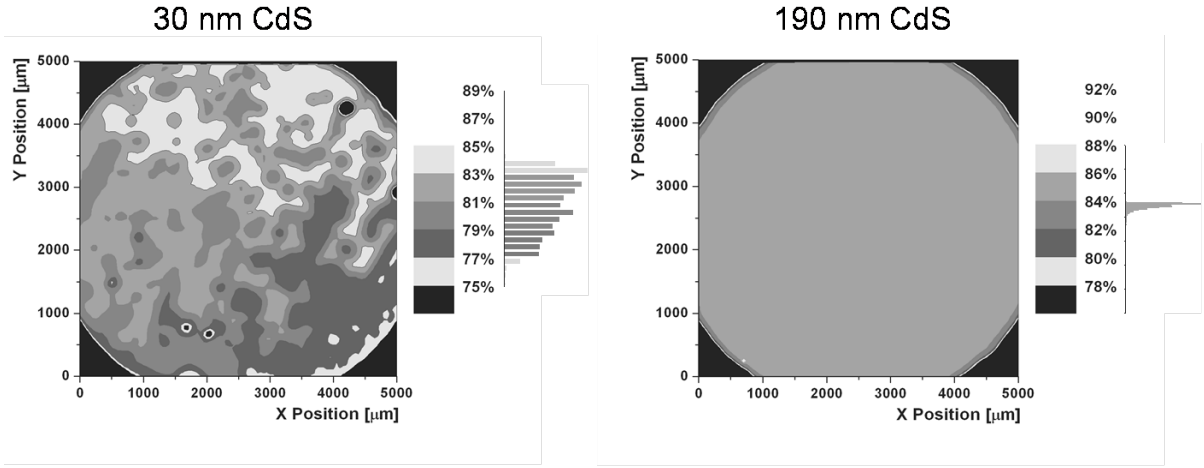

Figure 23. LBIC comparison of thin and intermediate-thickness CdS.

Photoluminescence (PL). Caroline Corwine, through a series of careful measurements in collaboration with Tim Gessert and others at NREL, has convincingly pinned down the physical origin of the key 1.456-eV PL line commonly seen with thin-film CdTe cells. Parts of this work were published in Appl. Phys. Lett. **86**, 221909 (2005) and presented at the Spring 2005 MRS Meeting.

The top two panels of Fig. 24 show the PL signal from CdTe cells made at NREL with and without the $CdCl_2$ processing step. Structure nearer the band gap is not shown, and it did vary between the two cells. However, the 1.456-eV line, and a series of its phonon replicas, was very similar between the two thin-film cases shown. Furthermore, the energy of this peak was quite constant as the excitation energy was varied by more than an order of magnitude. Such intensity-independence is a characteristic signature of a donor-to-band or band-to-acceptor transition. In this case the primary PL line implies an impurity level approximately 150 meV from one of the bands.

The procedure to identify the 1.456 line was to utilize single-crystal CdTe, where the line is not present, and expose a number of such samples to various etches, depositions, and annealing gasses. Special attention was given to the incorporation of copper, chlorine, and oxygen, since thin-film CdTe cells typically involve these elements during fabrication. The bottom panel of Fig. 24 is the result when a thin layer of copper was deposited, followed by annealing in oxygen. With this combination, the line of interest, the phonon replicas, and the intensity independence very closely replicate the thin-film spectra over the range shown. Other combinations of Cu, Cl, and O failed to match the thin-film results. Our opinion is that previous attribution of the 1.456 line to Cl defects neglected presence of Cu and O impurities in the cell fabrication process.

Identification of the specific Cu/O defect was assisted by first-principles band-structure calculations performed by Jingbo Li at NREL, which identified O_{Te}-Cu_i as the likely defect with an energy 125 meV below the conduction-band minimum. This assignment makes good physical sense in that when oxygen is present during annealing, it is likely to

substitute for Te, and when copper diffuses through CdTe, it is likely to so interstitially. Furthermore, the energetics should favor the O_{Te}-Cu_i complex over the individual defects.

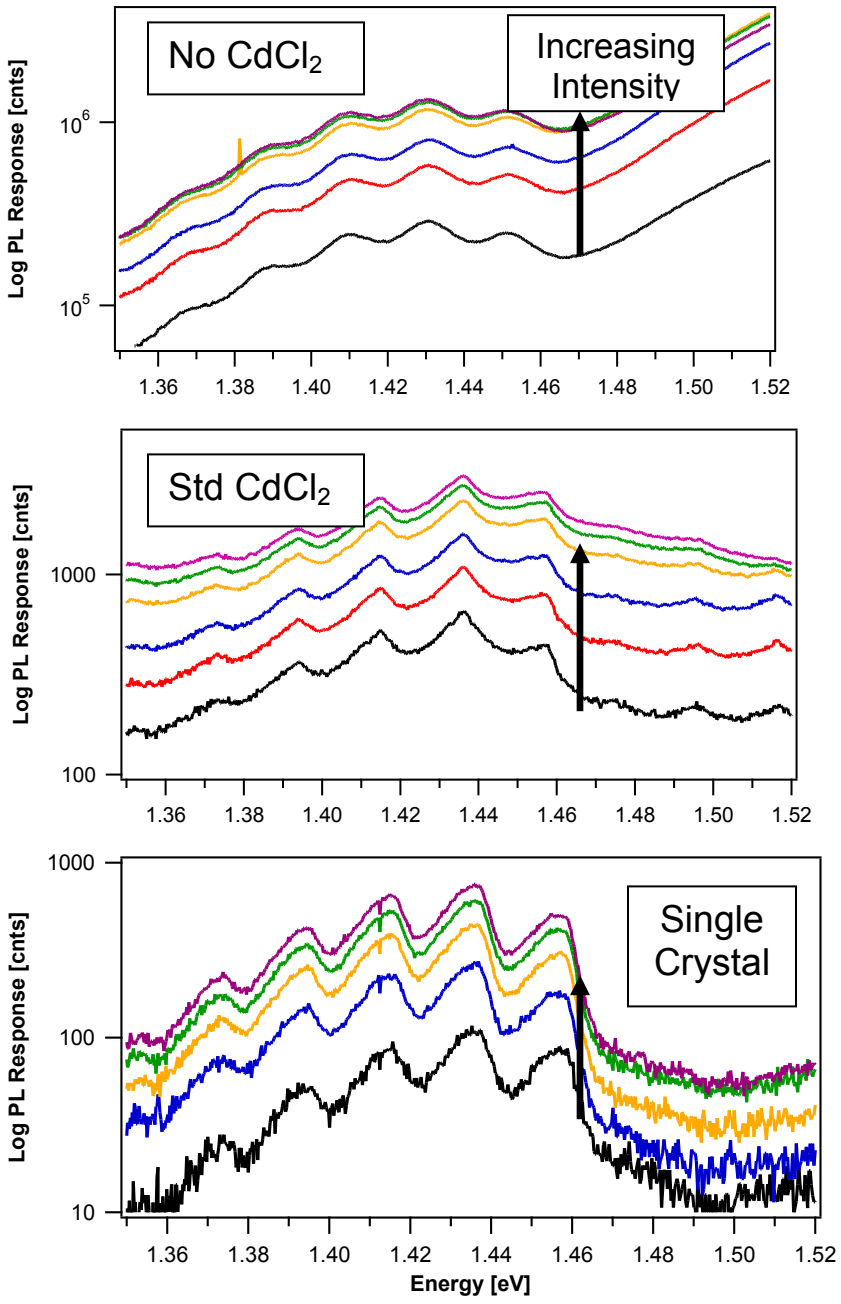

Figure 24. PL specta focused on the 1.456-eV peak and its phonon replicas. NREL cells (top, middle), single-crystal CdTe exposed to C and O (bottom).

Current Transients. Alan Fahrenbruch investigated the current transient response to voltage and illumination steps applied to CdS/CdTe cells. Results were presented at the

Spring 2005 MRS Meeting. The cells were obtained from Sampath at CSU, Gessert at NREL, and McCandless and Hegedus at IEC and included normal as well as abnormal devices. A typical result is shown in Fig. 25.

The initial measurement followed a dark soak at zero bias for several hours. All the cells showed dark forward-bias transients, but the magnitude and direction depended on cell preparation. In every case, the transients were reversible, and the recovery was not exponential, but was fit well by stretched exponentials (abbreviated SE in Fig. 26). Bias and light induced transients were small for the better behaved cells, those without rollover or cross-over, and the effect of these transients on efficiency was small. Abnormal devices with non-optimal Cu, however, showed much larger transients than those depicted in Fig. 25.

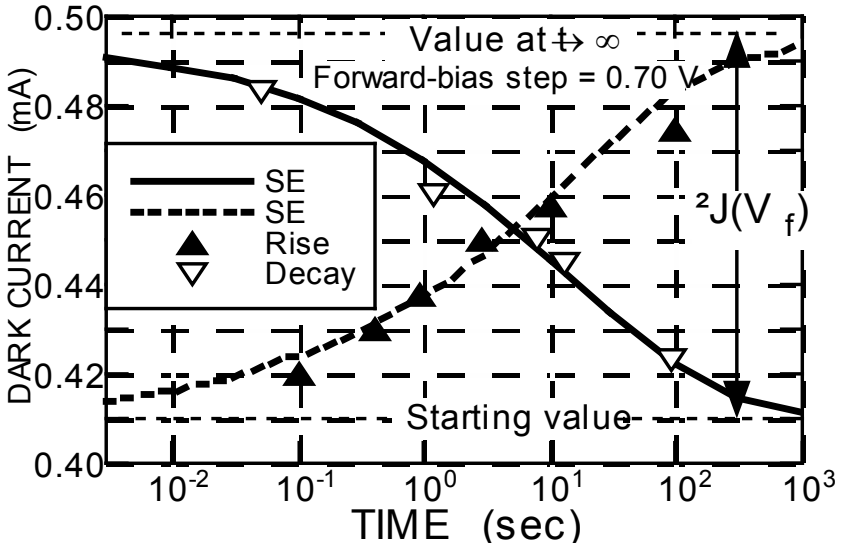

Figure 25. Transient current response following a positive or negative voltage step.

Similar transients have been observed by McMahon [Proc. 29th IEEE PV Specialists Conf., 2002, pp. 768-771] and by del Cueto and Osterwald [DOE Solar Program Review, 2004]. They have important implications for the measurement of cell efficiency and stability, and they provide clues about the current transport mechanisms. A possible mechanism involves modulation of the junction barrier profile by changing the charge on deep acceptors, giving a change in the effective junction barrier height.

GENERAL STUDIES

Non-uniformity Analysis. The relationship between small-area non-uniformities and performance at the module level is clearly important to PV technology. Ana Kanevce, Galym Koishiyev, and Marko Topič visiting from the University of Ljubljana in Slovenia have all contributed to this work. We found it important to first adopt a common terminology, and Figure 26 below gives a schematic representation of our general strategy.

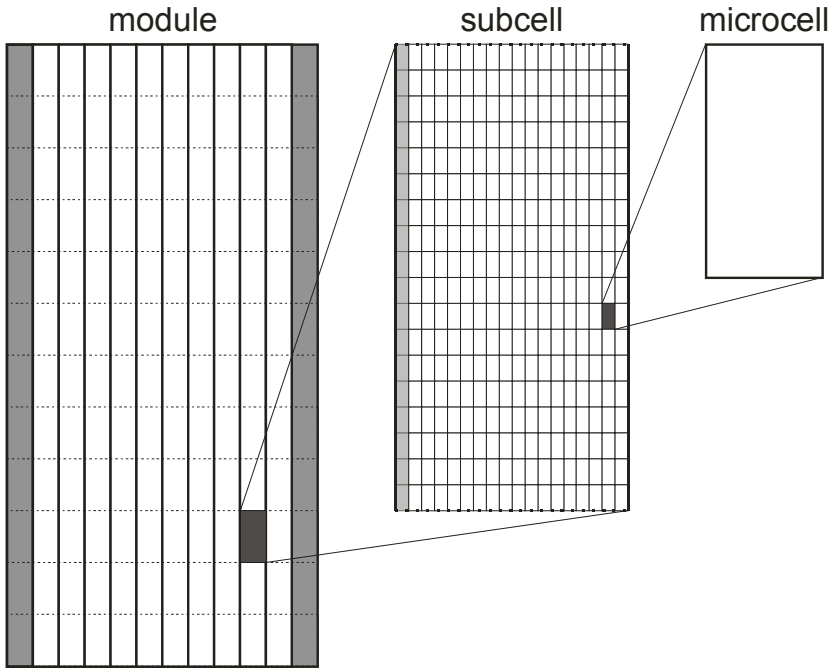

Figure 26. Terminology used for non-uniformity analysis.

The assumption is that most of a subcell, similar in size to a typical laboratory test cell, is uniform and consists of microcells with common, well-defined parameters. A subcell can be analyzed experimentally by LBIC down to the micron scale to determine the existence of small, but potentially troublesome, microcells consisting of local shunts, weak-diode areas, or areas of significantly reduced lifetime. In some cases, such defects can impact a much larger area than their physical extent. The combination of LBIC at different voltages and PSpice modeling appears to be sufficient to connect the parameters of the defective microcells with the J-V curve of the subcell. Such a J-V curve does not in

general follow a simple equation, and the PSpice result must be retained as a data file. It can, however, with a second level of PSpice modeling be used to calculate the J-V curve of the module and be used for direct comparison with the measured performance.

Physical non-uniformities of various types can also produce variations in the local photovoltage and shunting. For a non-uniform device, the equivalent circuit for a single diode can be replaced with a network of diodes that may be individually defined. Numerical simulations performed by Ana Kanevce used a 10 x 10 diode network, part of which is shown in Fig. 27. The CIGS baseline "strong diode" is 1 μm^2 in area and 17% efficient. The back-contact resistance was assumed to be negligible. The resistance R due to between the individual diodes in the array the transparent-conductive-oxide (TCO) front-contact should be proportional to the series resistance R_s of the solar cell as a whole. For the array illustrated here, an individual resistance of R = 3 Ω corresponds to series resistance of R_s = 1 Ω-cm^2 for the whole cell.

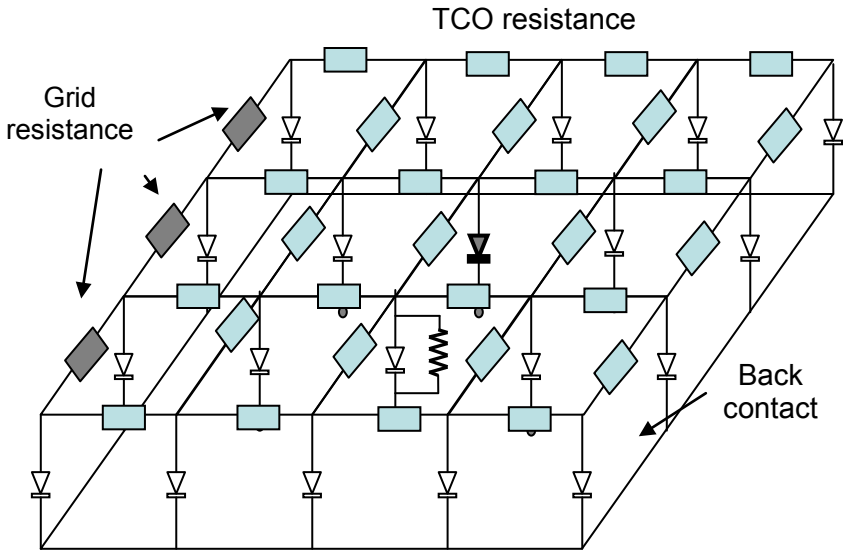

Figure 27. Schematic of diode network model. Single weak diode and shunt are highlighted.

If series resistance were neglected, a nonuniform device would be a network of parallel-connected diodes with no voltage drop between adjacent diodes. The total current generated by the device would be the sum of the currents through individual diodes:

$$I = \sum_{i=1}^{n}\left[I_{oi}\left(\exp\left(\frac{qV}{AkT} \right) - 1 \right) - I_{Li} \right]$$

The diode quality factor A was assumed to have the same value for all the diodes, and the light-generated current I_L was assumed to be uniform throughout the device. V_{oc} for the entire device is a function of the difference between the strong V_{ocs} and the weak-diode V_{ocw} voltage, $\Delta V_{oc} = V_{ocs} - V_{ocw}$, and of the ratio a of the weak-diode area A_w to the total device area A_t:

$$V_{oc} = V_{ocs} - \frac{AkT}{q}\ln\left[1 - a + a \cdot \exp\left(\frac{q\Delta V_{oc}}{AkT} \right) \right]$$

When series resistance is finite, J-V curves cannot be calculated analytically without approximation, but they can be calculated numerically. In the small R_s limit, numerical methods give the same results as those obtained analytically.

If TCO resistance is significant, it introduces a voltage drop across the TCO and thus isolates the lower-voltage area. Voltage maps $\Delta V(x,y) = V_S(x,y) - V_W(x,y)$ are shown in Fig. 28 for a small and a large value of R_S. $V_S(x,y)$ is the voltage of a uniform diode, and $V_W(x,y)$ is the voltage of 4% of the diodes with V_{oc} reduced by 0.4 V from its baseline value of 0.64 V. Although the sheet resistance in the TCO can isolate the weaker voltage areas and prevent them from dominating the entire device, it also reduces the fill-factor by a larger amount, and hence the cell's efficiency is always smaller when R_S is larger.

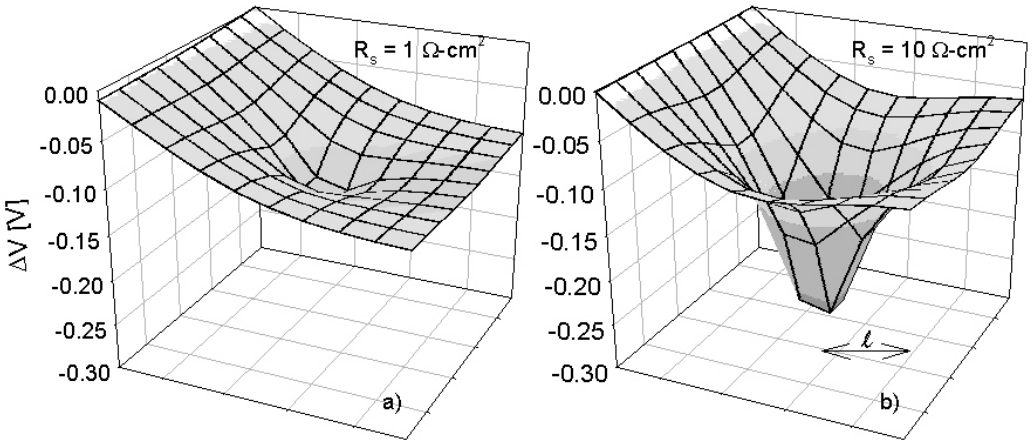

Figure 28. Voltage maps of two solar cells with different R_S. Length shown is often referred to as screening length.

The impact of a weak diode on device performance is linear in voltage and logarithmic in the area ratio to a first approximation. The calculated constant efficiency curves for a high-quality CIGS cell (17% baseline again) are shown in Fig. 29. Areas less than 10% of the total device area with voltage deficits less than 100 mV decrease the device efficiency less than 1% and can therefore be neglected.

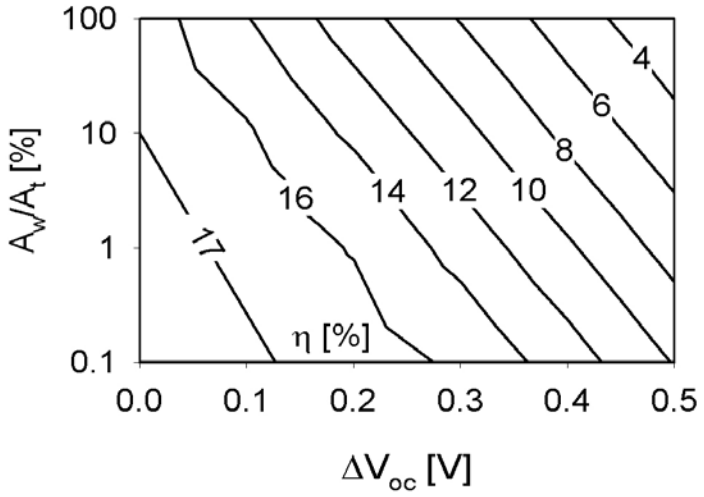

Figure 29. Efficiency dependence on ΔV_{oc} and weak area (baseline efficiency 17%).

Since the weak diodes pull down the voltage of the nearest neighbors, the distribution of the weak diodes, as well as their area and ΔV, could affect the device voltage. Calculations for a device with a total 4% weak-diode area showed the smallest voltage reduction when the diodes were clustered towards a corner of the device and the largest when they were scattered throughout the device. The maximum-power point, and thus the device efficiency, however, is nearly independent of the weak diodes' distribution.

Distributed Sheet Resistance. The single-value R_S used in Fig. 28 is an approximation of the distributed series resistance, which can yield J-V curves significantly different from the single-parameter approximation for the cell geometries commonly found in gridless thin-film modules. In general, the lateral voltage drop across the TCO layer requires a two-dimensional calculation. Such calculations have been done by Galym Koishiyev, also using PSpice and assuming a parallel array of small cells as shown in Fig. 30.

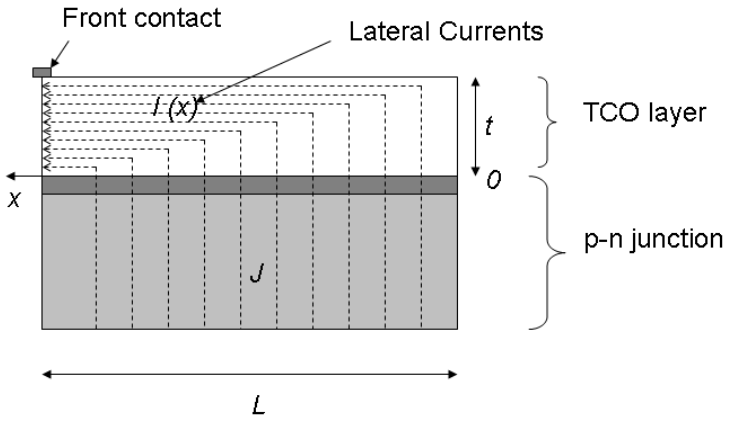

Figure 30. Current distribution in thin-film-module cell geometry.

Of significant practical interest is how the fill-factor of a module-geometry cell will change with TCO sheet resistance ρ_S and length L of the cell. Results with parameters corresponding to typical amorphous silicon cells, high-quality CIGS, and ideal solar cell are shown in Fig. 31 [submitted to SOLMAT]. When the resulting fill-factor is compared to that found in the absence of TCO resistance and is plotted against the dimensionless quantity $x = \rho_S L^2 J_{SC}/V_{OC}$, a nearly universal relationship is found. The value of x will be 0.5 or less for most practical situations. In this range the proportional fill-factor reduction will be nearly linear with sheet resistance, the square of cell length, and the J_{SC}/V_{OC} ratio. It will be slightly larger when a cell is closer to being ideal.

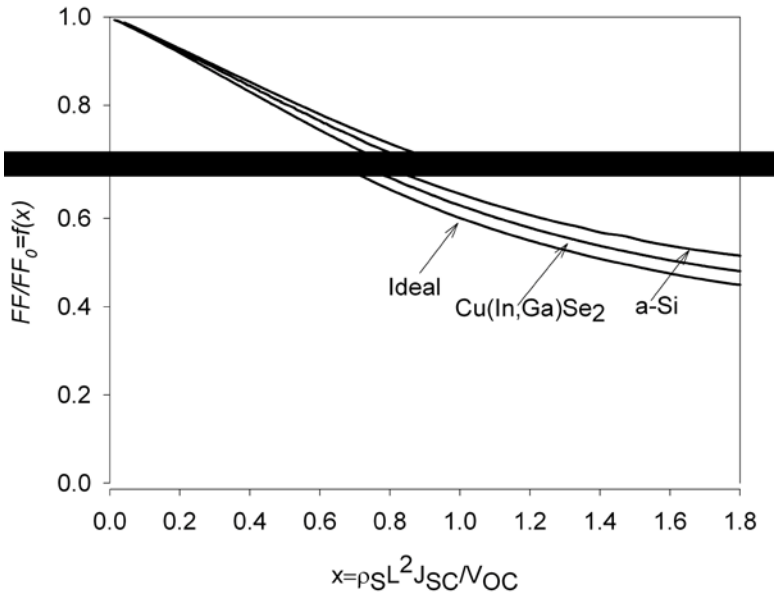

Figure 31. Quasi-universal dependence of fill-factor on module cell parameters.

Effective Module Efficiency. A joint project with Marko Topič and Kristijan Breel at the University of Ljubljana in Slovenia [Prog. in Photovoltaics, 2007] calculated the effective efficiency of PV modules averaged over a year under field conditions. In the absence of variations in temperature or illumination spectrum, and when the series resistance and the leakage conductance in a PV module are negligible, the module efficiency increases roughly logarithmically with solar irradiation. The primary variation is the open-circuit voltage V_{OC} and its direct effect on the fill-factor. The upper curve (a) in Fig. 32 shows the calculated efficiency vs. irradiance dependence for a Wurth Solar CIGS module based on the manufacturer's data sheets. The other three curves in Fig. 32 show the modifications to curve (a) as the module's temperature coefficient, effective series resistance, and effective leakage conductance are sequentially added to the calculation.

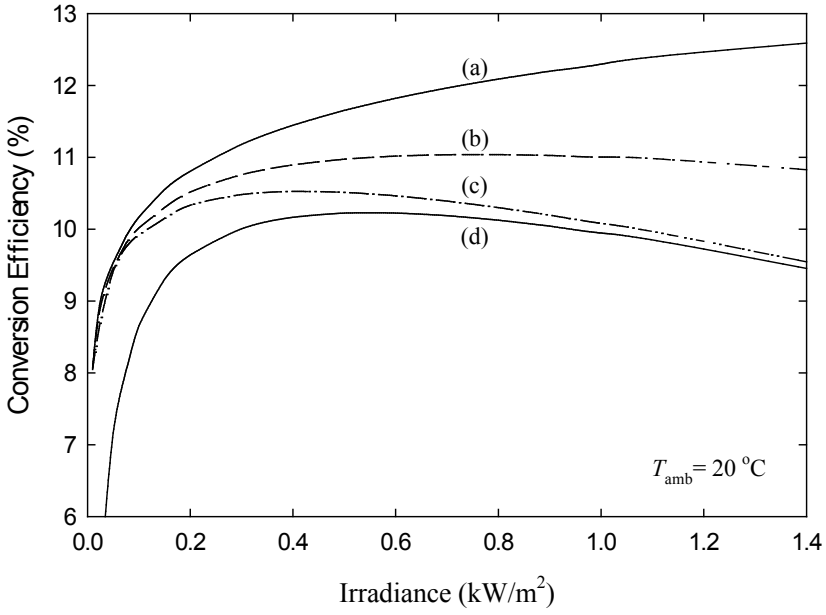

Figure 32. Dependence of conversion efficiency on irradiance for a Wurth CIGS module. (a) Constant cell temperature, (b) cell temperature proportional to irradiance, (c) addition of series resistance, and (d) addition of leakage conductance.

The increase in module temperature with irradiance, compared to the ambient temperature, is generally very linear and has essentially the same rate for a wide range of technologies. This temperature coefficient dT_c/dP is approximately 30ºC/kW-m^{-2}. The temperature effect (curve (b) in Fig. 32) therefore reduces $\eta(P)$ by an amount nearly

proportional to irradiance. The effective series resistance R_s per cell and the effective leakage conductance G_{sh} were deduced for Wurth Solar's WS75 modules. Curve (c) demonstrates that R_s has a larger effect at higher irradiance. G_{sh} per cell, on the other hand, reduces the module efficiency in inverse proportion to irradiance. Using $G_{sh} \cong 1$ mS/cm^2 deduced from the slopes of current-voltage characteristics at low voltages, curve (d) is calculated. The overall result is that the maximum efficiency for this module should occur in the neighborhood of one-half sun ($\eta = 10.2$ % at $P = 580$ W/m^2). The details of the curves shown in Fig. 32 will vary with the technology employed and with the values of dT_c/dP, δ, effective R_s and G_{sh} for the specific module fabricated, but the general form of such curves will be similar to those of Fig. 32. The simulation of the a-Si and CdTe modules was slightly more complicated than for CIGS, because the effective G_{sh} increased significantly with irradiance.

The annual effective efficiency η_{eff} can be calculated as a ratio of integrated available electrical energy generated in a year divided by the integrated solar energy. The process formally requires site-specific temperature and irradiance data, but the result does not depend strongly on the site selected. In general, η_{eff} is smaller η_{STC}, the often-specified efficiency corresponding to one sun and 25°C, and the ratio can vary as much as 10% among modules. We conclude that an approximate value of η_{eff}, the module efficiency at one-half sun, should be considered as a suitable parameter for comparing module output.

Barrier Heights. Graduate student Galym Koishiyev has developed relatively straightforward J-V analysis techniques to determine two types of barrier heights: the hole barrier due to the back contact and the electron barrier between window and absorber. In the first case, where current is limited above V_{OC}, we determine the current at which the J-V curve changes from positive to negative curvature. In the data from a CIGS cell fabricated by Neelkanth Dhere's group at FSEC (Fig. 33), this transition occurs at approximately 20 mA/cm^2 for the highest temperature shown and at about 0.5 for the lowest. This "turning current" J_t can then be plotted as a function of temperature and compared with an analytical expression for the hole barrier height.

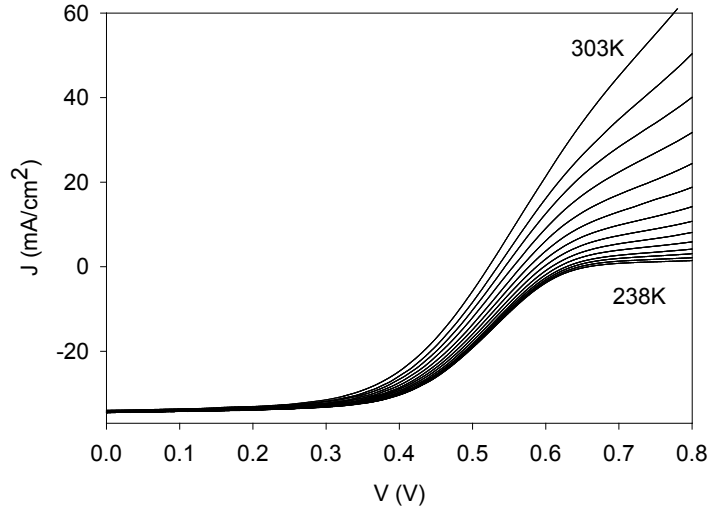

Figure 33. Effect of back-contact barrier on CIGS J-V.

When a series of curves is generated with barrier height as the free parameter (Fig. 34), J_t follows the curve for 0.44-eV barrier height reasonably well over a significant temperature range.

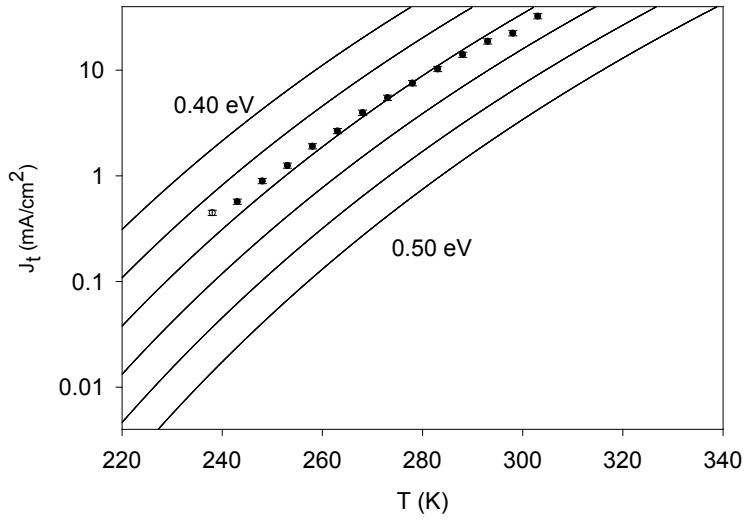

Figure 34. Turning current from Fig. 33 overlaid on that calculated from different barrier heights.

A similar approach (not shown here) for the second type of barrier, the electron barrier resulting from the conduction-band offset at the window/absorber interface, uses the crossover current between dark and light J-V curves. In this case, the plot of experimental crossover current is compared with analytical curves where the electron

barrier is the free parameter. The cells used to test this analysis were CdS/$CuInS_2$, and they also were fabricated at FSEC [results presented at the 33rd PVSC].

An additional strategy to determine barrier heights was pursued by Alan Fahrenbruch. He used simple optics and electronics to measure internal photoemission (IPE) in CdTe cells by plotting current response to sub-band-gap light vs. the photon energy. According to the Fowler theory, the energy intercept is equal to the barrier height. Alan looked at a number of CdTe cells from various fabricators, including those with good and bad contacts and electronically thick and thin cells. An example is given in Fig. 35.

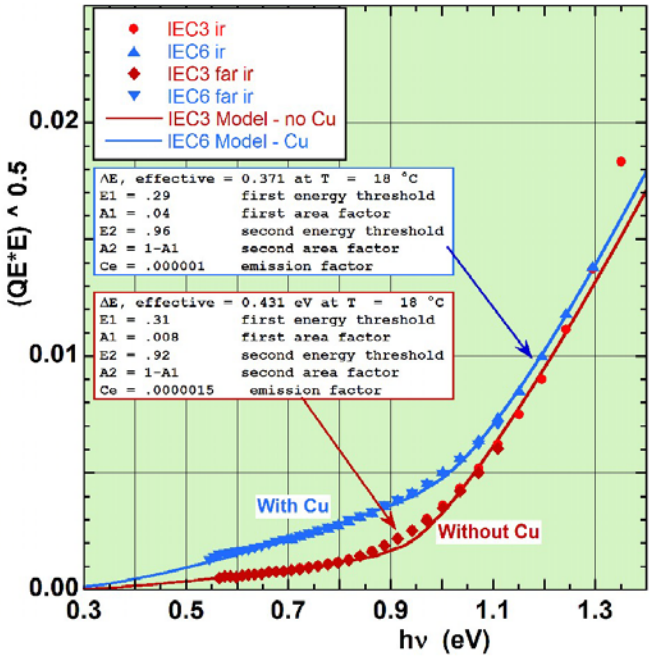

Figure 35. $(QE)^{0.5}$ vs. hν for IEC6 cell (with Cu) and IEC3 (without Cu) at 18°C. Points are measured data and curves are for model.

Alan's results suggest two barriers in parallel: a high one, (~ 0.9 eV) which agrees well with the observed UPS values and a low one (~ 0.3 eV) with a much smaller area fraction (1 - 4%) which dominates the contact transport and corresponds more closely to the values observed for efficient cells. For thick cells, his IPE results agree well with thermal measurements described above.

LBIC Measurements. LBIC measurements by Tim Nagle and Alan Davies have continued to provide a direct link between the spatial non-uniformities inherent in thin-film polycrystalline solar cells and the overall performance of these cells. LBIC is uniquely equipped to produce quantitative maps of local quantum efficiency with relative ease. In our system, spatial resolution of 1 μm at 1-sun intensity, and return to the same location after cell other measurements, is routinely achieved. The LBIC measurements demonstrate that several types of effects that alter cell performance can be traced to specific local-area features. Examples of such effects include defects related to edges, grids, or scribes, spatial variations in alloying, and local changes due to high-temperature stress. A summary of the CSU LBIC work was presented at the January 2005 PVSC in Orlando [J.R. Sites and T.J. Nagle, Proc. IEEE Photovoltaics Specialists Conf. **31**, 199-204 (2005)].

We have had a wavelength range of 638 to 857 nm available with a set of five diode lasers operated at room temperature. The 857 nm laser has been particularly useful, since it can be tuned to lower wavelengths by reducing its temperature and hence it can be scanned through the CdTe band gap. The scanning process has been made substantially easier during the past year with the construction of a control system based on a Stirling cooler by undergraduate Wolfgang Timko during a summer internship. Other recent upgrades have included better signal-to-noise electronics for operation under voltage bias, new mounting stages that allow cell transport to other measurement stations, and more sophisticated analysis software.

QE Under Light Bias. During the Subcontract, we very carefully recalibrated our quantum-efficiency system, refined the software and procedures for efficient data collection, and installed the capability a white-light bias of variable intensity. Much of the QE improvement was done by an undergraduate student, Jacob van der Vliet, who compared several reference-cell candidates and made cross-calibrations with reference cells measured at NREL. He also made several improvements to the QE measurement protocol and several upgrades to the software used to store and display the QE results.

Additionally, Tim Nagle and Alan Davies investigated different light sources and controls to apply white bias light during QE measurement. As with other researchers, they found that the QE curve can be affected by the presence of bias light. In many cases as shown in Fig. 36, the change is small, it only affects QE near the band gap, and it saturates with a modest amount of bias light. Nevertheless, it is a real effect that is quite reproducible. Its likely explanation for the Cds/CdTe cell shown is that there is a secondary effect from CdS photoconductivity, which leads to a small increase in the CdTe depletion width under illumination and hence improves the collection of electrons generated deep in the CdTe.

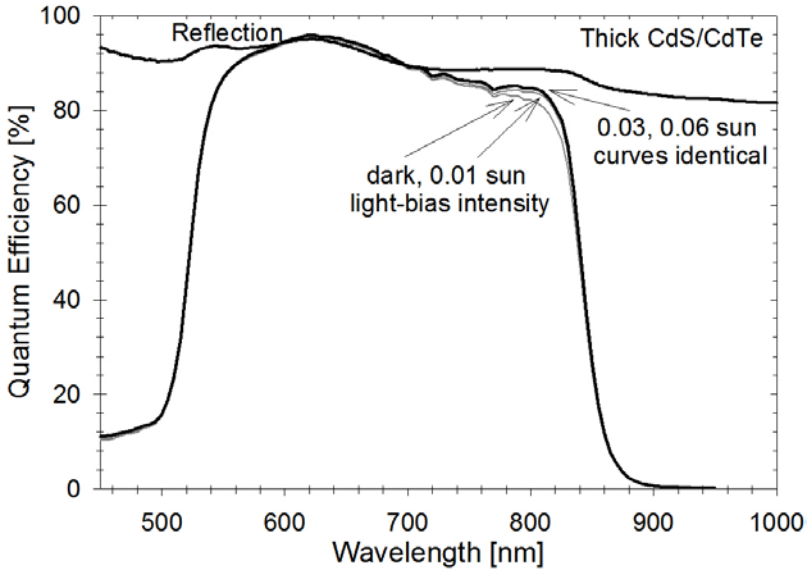

Figure 36. Small bias-light effect on measured CdS/CdTe QE.

In some cases, however, the effect of bias light can be much more dramatic. For example, a poor-efficiency CIGS yielded the QE curves shown in Fig. 37. The light-bias effect in this case was very large and was not saturated at 5% of standard solar intensity. The J-V curve (inset) suggests a large conduction-band offset ("spike") at the CdS/CIGS interface. Such a barrier would block photogenerated electrons unless there are sufficient blue photons absorbed in the CdS to lower the interfacial barrier.

For stronger bias light, we found that six-volt krypton "Mag-lite" bulbs are a suitable white-light source with an intensity that can be varied up to half a sun. Furthermore, they

are small enough to be mounted in our QE system without extensive modification. Simon Kocur, a visiting student from Regensburg, Germany, designed and built a mounting arrangement for Mag-lite bulbs so that the bulb-to-cell distance can now be varied over a sufficient range that light-bias intensity can be reproducibly varied from 1% to 50% of solar intensity.

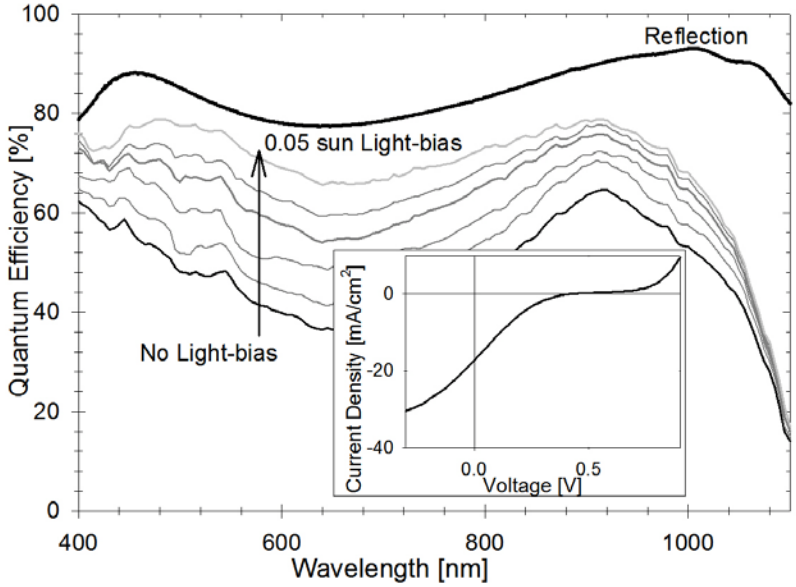

Figure 37. Strong QE dependence on bias-light suggests a large secondary barrier in the CdS/CIGS conduction band, an observation supported by the J-V curve.

COLLABORATIONS

During the Subcontract, we worked with CIGS industrial partners ISET, Heliovolt, Nanosolar, Solyndra, Miasole, and SoloPower, as well as CdTe partner AVA, in three primary areas: (1) measurement and analysis of specific cells in our lab, (2) advice for building or refining in-house systems for J-V, QE, and LBIC measurements, and (3) transfer of analysis and simulation software and consultation on its use. In general, the results of our work were reported to the companies without public dissemination.

Work with university partners at Aoyama Gakuin University, the University of Ljubljana, FSEC, and Sampath's group at Colorado State, as well as with NREL, was included in earlier sections.

In addition to the barrier-height analysis made with FSEC cells, however, we made QE, capacitance, and LBIC measurements on several selenide and sulfide cells fabricated at FSEC. These results were included in the FSEC presentation at the May 2008 PVSC, where Galym Koishiyev was a co-author. Similarly, Alan Davies collaborated with Victor Plotnikov at the University of Toledo and co-authored Victor's May 2008 PVSC presentation. The Toledo presentation included Alan's measurements and interpretation from a set of Toledo CdS/CdTe cells fabricated with a wide range of CdS thicknesses.

COMMUNICATIONS AND EDUCATION

Publications

1. A.O. Pudov, A. Kanevce, J.R. Sites, F. Hasoon, and H. Al-thani, "Impact of Conduction-Band Barrier on CdS/Cu(In,Ga)Se_2 Solar-Cell Performance," J. Appl. Phys, **97**, 064901 (2005).

2. M. Gloeckler and J.R. Sites, "Efficiency Limitations for Wide-Band-Gap Chalcopyrite Solar Cells," Thin Solid Films, **480-481**, 241-245 (2005).

3. A.O. Pudov, "CIGS J-V Distortions in the Absence of Blue Photons," Thin Solid Films, **480-481**, 273-278 (2005). With A.O. Pudov, M.A. Contreras, T. Nakada, and H.-W. Schock.

4. S.H. Demtsu and J.R.Sites, "Quantification of Losses in thin-film CdS/CdTe Solar Cells," Proc. IEEE Photovoltaic Specialists Conf. **31**, 347-350 (2005).

5. J.R. Sites and T.J. Nagle, "LBIC Analysis of Thin-Film Polycrystalline Solar Cells," Proc. IEEE Photovoltaics Specialists Conf. **31**, 199-204 (2005).

6. M. Gloeckler and J.R. Sites, "Band-Gap Grading in Cu(In,Ga)Se_2 Solar Cells," J. Phys. Chem. Solids, **66**, 1891-1894 (2005).

7. C.R Corwine, J.R. Sites, T.A. Gessert, W.K. Metzger. P. Dippo, J. Li, A. Duda, and G. Teeter, "CdTe Photoluminescence: Comparison of Solar-Cell Material with Surface-Modified Single Crystals," Appl. Phys. Lett. **86**, 221909 (2005).

8. M. Gloeckler, J.R. Sites, and W.K. Metzger, "Grain-Boundary Recombination in Cu(In,Ga)Se_2 Solar Cells," J. Appl. Phys. **98**, 113704, (2005).

9. M. Gloeckler and J.R. Sites, "Potential of Sub-micrometer Thickness Cu(In,Ga)Se_2 Solar Cells," J. Appl. Phys. **98**, 103703, (2005).

10. A. Kanevce, M. Gloeckler, A. Pudov, and J.R. Sites. "Conduction-Band Offset Rule Governing J-V Distortion in CdS/CI(G)S Solar Cells," Mat. Res. Soc. Proc. **865**, 221-226 (2005).

11. C. R. Corwine, J.R. Sites, T.A. Gessert, W.K. Metzger, P. Dippo, J. Li, A. Duda, and G. Teeter. "Photoluminescence Studies on Cu and O Defects in Crystalline and Thin-Film CdTe," Mat. Res. Soc. Proc. **865**, 197-202 (2005).

12. M. Gloeckler, J.R. Sites, and W.K. Metzger, "Simulation of Polycrystalline Cu(In,Ga)Se_2 Solar Cells in Two Dimensions," Mat. Res. Soc. Proc. **865**, 381-386 (2005).

13. S.H. Demtsu, D.S. Albin, J.Pankow, and A. Davies, "Stability Study of CdS/CdTe Solar Cells made with Ag and Ni Back-Contacts," Solar Energy Mat. Solar Cells **90**, 2934-2943 (2006).

14. A.L. Fahrenbruch, "Current Transients in CdS/CdTe Solar Cells," Mat. Res. Soc. Proc. **865**, 355-360 (2005).

15. S.H. Demtsu, and J.R. Sites, "Effect of Back-Contact Barrier on Thin-Film CdTe Solar Cells," Thin Solid Films, Thin Solid Films **510**, 320-324 (2006).

16. J. Pan, M. Gloeckler, and J.R. Sites, "Hole-Current Impedance and Electron-Current Enhancement by Back-Contact Barriers in CdTe Cells," J. Appl. Phys. **100**, 124505, (2006).

17. M. Topič, K. Breel and J.R. Sites. "Performance Assessment of PV Modules – Relationship Between STC Rating and Field Performance," Proc. World Conf. on Photovoltaic Energy Conversion **4**, 2141-2144 (2006).

18. A.L. Fahrenbruch, "The Relationship of CdS/CdTe Band Profiles to J-V Characteristics," Proc. World Conf. on Photovoltaic Energy Conversion **4**, 376-379 (2006).

19. S.H. Demtsu, D.Albin, and J.R. Sites, "Role of Copper in the Performance of CdS/CdTe Solar Cells," Proc. World Conf. on Photovoltaic Energy Conversion **4**, 523-526 (2006).

20. M. Topič, K. Brecl, J. Kurnik, and J. Sites, "Effective Efficiency and Performance Ratio as Energy Rating System for PV Modules," Proc. E-PVSEC **21**, 2507-2510 (2006).

21. D.S. Albin, S.H. Demtsu, and T.J. McMahon, "Film Thickness and Chemical Processing Effects on the Stability of CdTe Solar Cells," Thin Solid Films **515**, 2659-2668 (2006).

22. R. N. Bhattacharya, M.A. Contreras, B. Egaas, R. Noufi, and A. Kanevce, and J.R. Sites. "High Efficiency Thin Film $CuIn_{1-x}Ga_xSe_2$ Photovoltaic Cells Using a $Cd_{1-x}Zn_xS$ Buffer Layer," Appl. Phys. Lett. **89**, 253503, (2006).

23. M. Topič, K. Breel, and J.R. Sites, "Effective Efficiency of Photovoltaic Modules Under Field Conditions," Progress in Photovoltaics **15**, 19-26 (2007).

24. J.R. Sites and J. Pan, "Strategies to Increase CdTe Solar-Cell Voltage," Thin Solid Films **515**, 6909-6102 (2007).

25. A.R. Davies, J.R. Sites, A.E. Enzenroth, W.S. Sampath, and K.L. Barth. "All-CSS Processing of CdS/CdTe Thin-Film Solar cells with Thin CdS Layers," Proc. Mat. Res. Soc. **1012**, 157-162 (2007).

26. A. Kanevce and J.R. Sites, "Impact of Nonuniformities on Thin Cu(In,Ga)Se_2 Solar-Cell Performance," Proc. Mat. Res. Soc. **1012**, 293-298 (2007).

27. T.J. Nagle, A.R. Davies, and J.R. Sites, "Quantum-Efficiency Measurements to Deduce Non-Ideal Solar-Cell Features," Proc. Mat. Res. Soc. **1012**, 355-360 (2007).

28. A.L. Fahrenbruch, "Exploring Back-Contact Technology to Increase CdS/CdTe Solar-Cell Efficiency," Proc. Mat. Res. Soc. **1012**, 283-290 (2007).

29. S.H. Demtsu, D.S. Albin, J.R. Sites, W.K. Metzger, and A. Duda. "Cu-Related Recombination in CdTe Solar Cells," Thin Solid Films **516**, 2251-2254 (2008).

30. A.R. Davies and J.R. Sites, "Effects of Non-Uniformity on Rollover Phenomena in CdS/CdTe Solar Cells," Proc. Photovoltaics Specialists Conf. **33** (2008).

31. G.T. Koishiyev, J.R. Sites, S.S. Kulkarni, and N.G. Dhere, "Determination of Back Contact Barrier Height in Cu(In,Ga)$(Se,S)_2$ and CdTe Solar Cells," Proc. Photovoltaics Specialists Conf. **33** (2008).

32. A.L. Fahrenbruch, "Measuring CdS/CdTe Back-Contact Barrier Heights by Internal Photoemission," Proc. Photovoltaics Specialists Conf. **33** (2008).

33. G.T. Koishiyev and J.R. Sites, "TCO and Semiconductor Resistances in 2-D Modeling of Thin-Film Solar Cells," submitted to Solar Energy Materials and Solar Cells.

Presentations

1. Jim Sites, "LBIC Analysis of Thin-Film Polycrystalline Solar Cells," 31st Photovoltaics Specialists Conf., Orlando, January 2005.
2. Sam Demtsu, "Quantification of Losses in thin-film CdS/CdTe Solar Cells," 31st IEEE Photovoltaic Specialists Conf., Orlando, January 2005.
3. Markus Gloeckler, "Band-gap grading in CIGS Solar Cells," CIS Team Meeting, Golden, March 2005.
4. Jim Sites, "Alternative-Junctions Subteam Report," CIS Team Meeting, Golden, March 2005.
5. Jim Sites, "Photovoltaic Energy Conversion: The Big Picture," Colorado State University Physics Colloquium, April 2005.
6. Ana Kanevce, "Conduction-Band Offset Rule Governing J-V Distortion in CdS/CI(G)S Solar Cells," Mat. Res. Soc., San Francisco, April 2005.

7. Alan Fahrenbruch, "Current Transients in CdS/CdTe Solar Cells," Mat. Res. Soc. San Francisco, April 2005.
8. Caroline Corwine, "Photoluminescence Studies on Cu and O Defects in Crystalline and Thin-Film CdTe," Mat. Res. Soc., San Francisco, April 2005.
9. Markus Gloeckler, "Simulation of Polycrystalline Cu(In,Ga)Se_2 Solar Cells in Two Dimensions," Mat. Res. Soc., San Francisco, April 2005.
10. Alan Fahrenbruch, "Influence of Band Profiles on Transport and Recombination," CdTe Team Meeting, Golden, May 2005.
11. Jim Sites, "CdTe Solar Cells: Basic Model and Common Deviations," CdTe Team Meeting, Golden, May 2005.
12. Sam Demtsu, "Stability of CdS/CdTe Solar Cells with Ag and Ni Back Contacts," CdTe Team Meeting, Golden, May 2005.
13. Caroline Corwine, "Luminescence Studies on Cu and O Defects in Single-Crystal and Thin-Film CdTe," CdTe Team Meeting, Golden May 2005.
14. Jim Sites, "Potential for Submicron-Thickness CIGS Absorbers," Solar Energy Review Meeting, Denver, November 2005.
15. Jim Sites, "Thin-Film Polycrystalline Solar Cells: The Potential and the Challenges," Stanford University, January 2006.
16. Jim Sites, "Thin-Film Polycrystalline Solar Cells: The Potential and the Challenges," Nanosolar, Palo Alto, January 2006.
17. Jim Sites, "Device Physics and Numerical Simulation: Routes to Understanding CdTe and CIGS Cells," University of Delaware, February 21, 2006.
18. Jim Sites, "Basic Solar-Cell Measurements," Heliovolt Corporation, Austin, TX, March 1, 2006.
19. Jim Sites, Jun Pan, and Markus Gloeckler, "Impact of Lifetime and Back-Contact Barrier on CdTe Current-Voltage Curves: Simulation of Commonly Seen Features," CdTe Team Meeting, Golden, March 9, 2006.
20. Alan Davies, "Effect of Cu and $CdCl_2$ on Stability," CdTe Team Meeting, Golden, March 9, 2006.
21. Caroline Corwine, "Compensating Cu/O Complex in CdTe," CdTe Team Meeting, Golden, March 9, 2006.
22. Alan Fahrenbruch, "Photoconductive CdS and Anomalous QE Effects: Comparison of Experiment and Modeling," CdTe Team Meeting, Golden, March 9, 2006.
23. Jim Sites, "Can V_{OC} in CdTe Cells Be Increased Significantly?" CdTe Team Meeting, Golden, March 10, 2006.
24. Markus Gloeckler, "Potential for Thin-Film CIGS: a Device Study," CIS Team Meeting, Golden, April 6, 2006.
25. Ana Kanevce, "Predicted Behavior of Cells with Thin CIGS Absorbers," CIS Team Meeting, Golden, April 6, 2006.
26. Alan Fahrenbruch, "The Relationship of CdS/CdTe Band Profiles to J-V Characteristics," WCPEC-4, Kona, Hawaii, May 12, 2006.
27. Jim Sites and Jun Pan, "Strategies to Increase CdTe Solar-Cell Voltage," E-MRS, Nice, France, May 31, 2006.

28. Jim Sites, "Why are There Large Differences in CdTe J-V Curves?" SOLARPACT Meeting, Nice, France, June 2, 2006.
29. Jim Sites, "CIGS: Four Grain-Boundary Possibilities," Grain-Boundary Workshop, Frejus, France, June 3, 2006.
30. Jim Sites, "Device Physics and Numerical Simulation: Routes to Understanding CIGS and CdTe," University of Ljubljana, Slovenia, July 6, 2006.
31. Jim Sites, "Photovoltaic Energy Conversion: The Big Picture," Ball Aerospace, Boulder, March 16, 2007.
32. Alan Fahrenbruch, "Exploring Back-Contact Technology to Increase CdS/CdTe Solar-Cell Efficiency," MRS Meeting, San Francisco, April 12, 2007.
33. Jim Sites, "Device Physics of Thin-Film Polycrystalline Solar Cells," Organic and Nanostructure Electronics Workshop, Montreal, May 17, 2007.
34. Jim Sites, "Photovoltaics: The Big Picture," Osher Foundation Public Lecture, Fort Collins, November 8, 2007.
35. Jim Sites, "Photovoltaic Energy Conversion," Global-Warming Symposium, Colorado State University, November 13, 2007.
36. Jim Sites, "Voltage Limitations for CdTe and CIGS Solar Cells," Photovoltaic Science and Engineering Conference, Fukuoka, Japan, December 4, 2007.
37. Jim Sites, "Device Physics of Thin-Film Solar Cells," Industrial Technology and Research Institute, Hsinshu, Taiwan, December 10, 2007.
38. Jim Sites, "Thin-Film Solar Cells, The Potential and the Challenge," Taiwanese Photovoltaic Association, Hsinshu, Taiwan, December 11, 2007.
39. Jim Sites, "Materials Studies in Physics at CSU with Emphasis on Thin-Film Solar Cells," J. Nehru Center, Bangalore, India, January 15, 2008.
40. Jim Sites, "CIGS Cells and Manufacturing in the US," Future Directions in Photovoltaics Workshop, Tokyo, March 7, 2008,
41. Jim Sites, "Device Physics of Polycrystalline Thin-Film Solar Cells," Aoyama Gakuin Univerisity, Tokyo, March 8, 2008.
42. Jim Sites, "Practical Information from Basic Photovoltaic Measurements," Beyond Conventional Silicon Workshop, Denver, June 18, 2008,
43. Jim Sites, "Photovoltaic Education at Colorado State University," PV Education Workshop, Boston, July 18, 2008.

PhD Degrees

1. Alex Pudov (PhD, May 2005), Thesis: "Numerical Modeling of CIGS Solar Cells: Definition of the Baseline and Explanation of Superposition Failure."

2. Markus Gloeckler (PhD, August 2005), Thesis: "The Effect of Trapping Defects on CIGS Solar-Cell Performance".

3. Caroline Corwine (PhD, August 2006), Thesis, "Role of Cu-O Defect in CdTe Solar Cells."

4. Samuel Demtsu (PhD, August 2006), Thesis: “Impact of Back-Contact Materials on the Performance and Stability of CdS/CdTe Solar Cells.”

5. Ana Kanevce (PhD, August 2007), Thesis: “Anticipated Performance of $Cu(In,Ga)Se_2$ Solar Cells in the Thin-Film Limit.”

6. Jun Pan (PhD, August 2007), Thesis: “Impact of Lifetime Variations and Secondary Barriers on CdTe Solar Cell Performance.”

7. Timothy Nagle (PhD, December 2007), Thesis: “Quantum Efficiency as a Device-Physics Interpretation Tool for Thin-Film Solar Cells.”

8. Alan Davies (PhD, August 2008), Thesis: “Effects of Contact-Based Non-Uniformities in CdS/CdTe Thin-Film Solar Cells.”

MS Degrees

1. Galym Koishiyev (MS, January 2007), coursework degree, now PhD candidate.

2. Lei Chen (MS, May 2008), Thesis, “Random Deposition Model of CdS Layer in CdS/CdTe Solar Cells.”

Other Students

1. Ray Hsiao, PhD candidate (2007 to present).

2. Wolfgang Timko, undergraduate intern (2005).

3. Jacob van Vliet, undergraduate researcher (2005).

4. Simon Kocur, undergraduate intern (2007).

5. Elisabeth Rengnath, undergraduate intern (2008).

REPORT DOCUMENTATION PAGE

Form Approved
OMB No. 0704-0188

PLEASE DO NOT RETURN YOUR FORM TO THE ABOVE ORGANIZATION.

1. REPORT DATE *(DD-MM-YYYY)*	2. REPORT TYPE	3. DATES COVERED *(From - To)*
January 2009	Subcontract Report	December 2004 - July 2008

4. TITLE AND SUBTITLE
Characterization and Analysis of CIGS and CdTE Solar Cells: December 2004 - July 2008

5a. CONTRACT NUMBER
DE-AC36-08-GO28308

5b. GRANT NUMBER

5c. PROGRAM ELEMENT NUMBER

6. AUTHOR(S)
J.R. Sites

5d. PROJECT NUMBER
NREL/SR-520-44811

5e. TASK NUMBER
PVB91199

5f. WORK UNIT NUMBER

7. PERFORMING ORGANIZATION NAME(S) AND ADDRESS(ES)
Colorado State University
Department of Physics
Fort Collins, Colorado 80523

8. PERFORMING ORGANIZATION REPORT NUMBER
XXL-5-44205-03

9. SPONSORING/MONITORING AGENCY NAME(S) AND ADDRESS(ES)
National Renewable Energy Laboratory
1617 Cole Blvd.
Golden, CO 80401-3393

10. SPONSOR/MONITOR'S ACRONYM(S)
NREL

11. SPONSORING/MONITORING AGENCY REPORT NUMBER
NREL/SR-520-44811

12. DISTRIBUTION AVAILABILITY STATEMENT
National Technical Information Service
U.S. Department of Commerce
5285 Port Royal Road
Springfield, VA 22161

13. SUPPLEMENTARY NOTES
NREL Technical Monitor: Bolko von Roedern

14. ABSTRACT *(Maximum 200 Words)*
The project goals have been to (1) reliably and quantitatively separate individual performance loss mechanisms, (2) expand the tools available for such measurement and analysis, (3) refine the physical explanations for performance losses, and (4) suggest fabrication approaches or modifications that can reduce these losses. A number of studies relating to the fundamental operation of CIGS and CdTe solar cells were performed during the subcontract period. In addition, we have expanded our light-beam-induced-current (LBIC) capabilities and the formalism needed to evaluate spatial nonuniformities, and we have analyzed the effective efficiency to be expected from commercial thin-film modules

15. SUBJECT TERMS
PV; solar cells; light-beam-induced current; copper indium gallium diselenide; cadmium telluride; grain boundary; two-dimensional modeling; back-contact barrier;

16. SECURITY CLASSIFICATION OF:			17. LIMITATION OF ABSTRACT	18. NUMBER OF PAGES	19a. NAME OF RESPONSIBLE PERSON
a. REPORT	b. ABSTRACT	c. THIS PAGE			
Unclassified	Unclassified	Unclassified	UL		19b. TELEPHONE NUMBER (*Include area code*)